Pathological and immunological characterization of bluetongue virus serotype 1 infection in type I interferons blocked immunocompetent adult mice

Mani Saminathan [a], Karam Pal Singh [a,*], Madhulina Maity [a], Sobharani Vineetha [a], Gundallhalli Bayyappa Manjunathareddy [b], Kuldeep Dhama [a,*], Yashpal Singh Malik [c], Muthannan Andavar Ramakrishnan [d], Jyoti Misri [e], Vivek Kumar Gupta [f]

[a] Division of Pathology, ICAR-Indian Veterinary Research Institute (ICAR-IVRI), Izatnagar, Bareilly 243122, Uttar Pradesh, India
[b] ICAR-National Institute of Veterinary Epidemiology and Disease Informatics, Bengaluru 560064, Karnataka, India
[c] College of Animal Biotechnology, Guru Angad Dev Veterinary and Animal Sciences University, Ludhiana 141001, Punjab, India
[d] Regional Station, ICAR-IVRI, Hebbal, Bengaluru 560024, Karnataka, India
[e] Animal Science Division, Indian Council of Agricultural Research, New Delhi 110001, India
[f] Centre for Animal Disease Research and Diagnosis, ICAR-IVRI, Izatnagar, Bareilly 243122, Uttar Pradesh, India

GRAPHICAL ABSTRACT
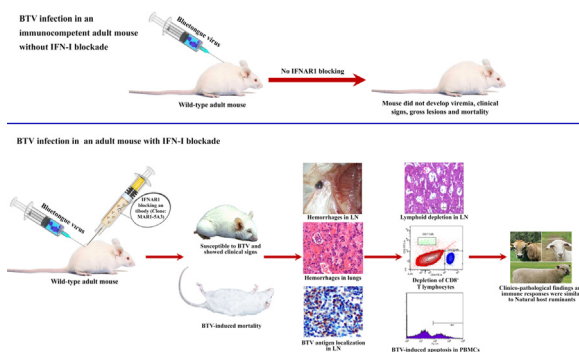
ARTICLE INFO

ABSTRACT

Introduction: Wild-type adult mice with intact interferon (IFN) system were neither susceptible to bluetongue virus (BTV) infection nor showed signs of morbidity/mortality. Establishment of immunologically competent wild-type adult mouse model with type I IFNs blockade is necessary to assess the pathogenesis, immune responses and testing of BTV vaccines.

Objectives: Present study aimed to establish and characterize BTV serotype 1 infection in immunocompetent adult mice with type I IFNs blockade at the time of infection by studying immune responses and sequential pathology.

Methods: Adult mice were administered with anti-mouse IFN-α/β receptor subunit-1 (IFNAR1) blocking antibody (Clone: MAR1-5A3) 24 h before and after BTV serotype 1 infection, and sacrificed at various time points. Sequential pathology, BTV localization by immunohistochemistry and quantification by qRT-PCR, immune cell kinetics and apoptosis by flow cytometry, and cytokines estimation by c-ELISA and qRT-PCR were studied.

Peer review under responsibility of Cairo University.

* Corresponding authors.

E-mail addresses: karam.singh@rediffmail.com (K.P. Singh), kdhama@rediffmail.com (K. Dhama).

Results: IFNAR blocked-infected mice developed clinical signs and typical lesions of BT; whereas, isotype-infected control mice did not develop any disease. The IFNAR blocked-infected mice showed enlarged, edematous, and congested lymph nodes (LNs) and spleen, and vascular (congestion and hemorrhage) and pneumonic lesions in lungs. Histopathologically, marked lymphoid depletion with "starry-sky pattern" due to lymphocytes apoptosis was noticed in the LNs and spleen. BTV antigen was detected and quantified in lymphoid organs, lungs, and other organs at various time points. Initial leukopenia (increased $CD4^+/CD8^+$ T cells ratio) followed by leukocytosis (decreased $CD4^+/CD8^+$ T cells ratio) and significantly increased biochemical values were noticed in IFNAR blocked-infected mice. Increased apoptotic cells in PBMCs and tissues coincided with viral load and levels of different cytokines in blood, spleen and draining LNs and notably varied between time points in IFNAR blocked-infected mice.

Conclusion: Present study is first to characterize BTV serotype 1 infection in immunocompetent adult mouse with type I IFNs blockade. The findings will be useful for studying pathogenesis and testing the efficacy of BTV vaccines.

Introduction

Bluetongue (BT) is a non-contagious viral disease of domestic and wild ruminants caused by bluetongue virus (BTV), belongs to the genus *Orbivirus* and family *Reoviridae* [1,2]. Bluetongue virus is transmitted by biting midges of the genus *Culicoides* (family *Ceratopogonidae*) and has the ability to spread rapidly over long distances [1]. Direct economic losses associated with BTV are due to the high morbidity, mortality, abortions and fetal abnormalities. Indirect losses are due to international trade ban on animal movement, their products, and cost for treatment and control programs [1].

Bluetongue virus causes severe disease in sheep, characterized by pyrexia, serous to mucopurulent nasal discharge, edema of lips and face, cyanosis of tongue, oral erosions and ulcers, and lameness with hyperemia of coronary band [2–4]. In contrast, cattle and goats frequently exhibit sub-clinical or mild disease [4]. Contrarily, BTV-8 outbreaks in Europe during 2006 caused severe disease in cattle and goats [2,4]. As of now, 28 BTV serotypes have been reported and frequent genetic reassortments resulted in routine change in the global distribution of BTV serotypes and incursion of new BTV serotypes with high virulence into disease-free zones [1]. Among these, 23 BTV serotypes have been reported in India and BT acquired an endemic situation in India [1].

Natural hosts, sheep and cattle, are suitable models to study the pathogenesis, virulence, host-pathogen interaction, and testing of BTV vaccines. However, their use is restricted by stringent ethical issues, there is a difficulty in availing BTV sero-negative animals, animal cost, and their housing requires vector-proof specialized facilities [4–6]. To overcome these critical issues, finding a laboratory animal model, especially an adult mouse model, is necessary to facilitate studies on the pathogenesis, immune responses, and vaccine trials against BTV [7]. However, wild-type adult mice with an intact interferon (IFN) system are neither susceptible to BTV infection nor showed viremia/clinical signs/lesions/mortality when these mice were inoculated intravenously (I/V) or subcutaneously (S/C) with BTV [5–8]. Bluetongue virus is a 5–10 times more potent type I IFNs [interferon-alpha (IFN-α) and interferon-beta (IFN-β)] inducer (600,000 units/mL of plasma) in wild-type mouse after 8 h of infection [7–10]. The BTV infection in newborn mice through intracranial (I/C) route leads to severe cerebral lesions, which do not resemble the hemorrhagic, immunosuppressive and respiratory lesions observed during BT infection in natural host [7,11,12]. The BTV infection in 2-week-old mice resulted in mild disease due to limited viral replication, and BTV infection in 4-week-old mice did not cause clinical disease due to no viral replication [13]. All these studies suggested that absence of BTV infection in wild-type adult mice may be due to induction of abnormally excessive levels of type I IFNs resulted in brief and strong antiviral innate immune responses [5–8,10]. Calvo-Pinilla et al. [5] and Ortego et al. [6] have characterized an IFN-α/β receptor deficient [IFNAR$^{(-/-)}$] mouse model to study the BTV serotypes.

The present study was designed to establish the BTV infection in an immunocompetent adult mouse with temporary type I IFNs blockade, only induced at the time of infection using MAR1-5A3 monoclonal antibody. The remarkable advantages of this mouse model include easy availability, temporary immune deficiency, the disease is more natural, reversal to normal immune responses, increased virus replication, and resemblance to IFNAR$^{(-/-)}$ mice [7]. Recently, adult mice with temporal blockade of type I IFN receptors have been used as model to study the Zika virus, lymphocytic choriomeningitis virus, West Nile virus, and vesicular stomatitis virus infections [7,14–17]. The IFNAR blocked-infected mice might be useful for studying the BTV virulence, pathogenesis, transmission, host-virus interaction, immune responses against BTV rather than mortality, and testing the protective efficacy of BTV vaccines. The present study is the first to characterize the pathological, virological and immune responses in IFNAR blocked-BTV-infected adult mice.

Materials and methods

Animals

Female virgin 6–8 weeks old Swiss albino mice were procured from the Laboratory Animal Resource (LAR) Section, ICAR-Indian Veterinary Research Institute (ICAR-IVRI), Bareilly, India. Mice were maintained in polypropylene cages with ad libitum feed and water, and in an insect proof accommodation. Experiments were conducted by following the guidelines and regulations of Committee for the Purpose of Control and Supervision on Experiments on Animals (2003) and Institute Animal Ethics Committee, ICAR-IVRI, Bareilly [Approval No. F26-1/2015–16/JD(R)].

Blocking of type 1 IFN receptors and experimental design

To block IFNAR1 signaling without depleting the IFNAR1 bearing cells, wild-type mice (n = 30) were administered intraperitoneally (I/P) with 1.5 mg/mouse of anti-mouse IFN-α/β receptor (IFNAR1) monoclonal antibody (Clone: MAR1-5A3; Leinco Technologies, Inc., St. Louis, Missouri, USA) one day prior to BTV infection and with 0.5 mg/mouse one day after BTV infection (day −1 and day +1), as described previously [14–17]. On day 0, mice were injected I/V with a 50 µL volume containing 1×10^6 TCID$_{50}$/mL of BTV-1 and these comprised the IFNAR blocked-infected group (Supplementary Fig. 1). Mice (n = 27) were injected I/V with 50 µL of tissue culture medium without BTV and I/P with MAR1-5A3 antibody as described above and these comprised the non-infected control group. Mice (n = 27) were inoculated I/P with the same dose of mouse IgG isotype control one day prior to and

one day after BTV infection, as described above and acted as isotype-infected control group. The mice were daily monitored for 21 days post infection (dpi) for any clinical signs or mortality. Three mice each from the IFNAR blocked-infected, isotype-infected control and non-infected control groups were euthanized at 2, 3, 5, 7, 9, 12, 15, 18, and 21 dpi.

Inocula

The BTV serotype-1 (SKN-10/India/2007) used in this study was isolated from aborted fetal spleen of goats at Sardarkrushinagar, Gujarat, India [18]. The virus was passaged in BHK-21 and KC cells, titrated and BTV serotype was confirmed by following the protocol described previously by Saminathan et al. [17].

Clinical observations

Each mouse from different groups was monitored for individual clinical signs that are scored by following the modified method of Jabbar et al. [19] and Marin-Lopez et al. [20]. The following individual clinical signs were monitored: Activity: normal 0, slightly reduced 1, reduced 2 and severely reduced 3; Apathy: absent 0, mild 1 and marked 2; Hunched posture/huddling tendency: absent 0, mild 1 and marked 2; Ruffled or rough hair coat: absent 0, mild 1 and marked 2; Alopecia: absent 0, mild 1 and marked 2; Ocular and nasal discharges: absent 0, mild 1 and marked 2; Dyspnea/snuffling/chattering: absent 0, mild 1 and marked 2; Swelling around the eyes: absent 0, mild 1 and marked 2; and Weight loss: absent 0, mild 1 and marked 2. The final clinical score for each mouse was the sum of all the scores of clinical signs. The minimum score was 0 for healthy and 1 to 19 depending upon the severity of clinical signs.

Post-mortem lesions

Necropsy examination was conducted and gross lesions were recorded in inguinal and axillary lymph nodes (LNs), spleen, lungs, thymus, heart, liver, ovaries, uterus, and brain.

Sample collection

The control mice were necropsied first, to avoid cross-contamination and equipments were sterilized between the infected animals during sampling. During sacrifice, blood was collected from control and infected animals in EDTA coated vacutainers for hematology, BTV nucleic acid detection and quantification, fluorescent activated cell sorting (FACS), and cytokine gene expression studies. Blood was also collected for serum in BD Vacutainer™ plus plastic SST™ with Polymer Gel tubes (Becton Dickinson Pvt. Ltd., New Delhi, India) for biochemical analysis, BTV antibodies and cytokine levels estimation. Tissues from inguinal and axillary LNs, spleen, lungs, thymus, heart, liver, ovaries, uterus, and brain were preserved in 10% NBF for histopathology and immunohistochemistry (IHC), and in RNAlater™ (Invitrogen, ThermoFisher Scientific, New York, USA) for BTV and cytokine genes quantification, and stored at −80 °C. The spleen was preserved in RPMI-1640 medium for FACS analysis.

Histopathology

The formalin-fixed tissues were washed in water, dehydrated in ascending grades of alcohol, embedded in paraffin, and stained with hematoxylin and eosin (H&E) as per standard procedure.

RNA extraction

Total RNA was isolated from blood and various tissues using TRIzol™ reagent. The RNA was treated with DNase enzyme to eliminate the possible contamination of genomic DNA. The RNA purity was analyzed using spectrophotometry and its integrity was tested using electrophoresis.

Quantification of BTV genome by qRT-PCR

The viral load in blood and various tissues (draining LNs, spleen, thymus, lungs, heart, brain, ovaries, and uterus) from IFNAR blocked-infected and isotype-infected control groups at various intervals were quantified by Taqman probe-based quantitative reverse transcription PCR (qRT-PCR) using NS3 probe and primers (Supplementary Table 1) as described previously [17,21]. The PCR reaction mix (25 μL each) was made and the cycling conditions were followed as described previously by Saminathan et al. [17]. The cycling conditions were reverse transcription at 50 °C for 30 min, initial PCR activation at 95 °C for 15 min, template denaturation at 94 °C, primer annealing at 56 °C, extension at 72 °C for 30 sec, and final extension at 72 °C for 10 min. At the end of the reaction, dissociation curve was used for confirmation of qRT-PCR amplification. The standard curve was generated with an amplification efficiency of 101.61% and $R^2 = 0.996$ (y = -3.284x + 40.90) for the quantification of BTV nucleic acid in samples. The limit of quantification (LOQ) for the qRT-PCR assay was 35 copy numbers.

Immunohistochemistry

The BTV antigen was demonstrated in draining LNs, spleen, thymus, trachea, lungs, heart, liver, and brain by following the protocol described previously by Saminathan et al. [17]. Sections were incubated overnight with BTV primary antibody raised in rabbit (1:20 dilution) in a humidified chamber at 4 °C. The BTV infected tissues received identical treatment with the exception of primary antibody and acted as antibody control. The slides were incubated with goat anti-rabbit peroxidase-conjugated secondary antibody. The slides were incubated with DAB substrate and counter stained with Mayer's hematoxylin. Positive control slides were prepared from known BTV positive samples. The tissue sections from uninfected mice were treated identical to infected slides with BTV primary antibody at similar concentration and acted as negative control.

BTV specific antibody detection

The BTV antibodies were confirmed in the serum of non-infected and isotype-infected controls, and IFNAR blocked-infected mice using a BTV-VP7 c-ELISA Kit (VMRD Inc., Pullman, Washington, USA). The results were expressed as percentage inhibition values and equal to or more than 50% values were considered as positive as described previously by Saminathan et al. [17].

Hematology

The blood samples were analyzed for total leukocyte count (TLC), differential leucocyte count (DLC), red blood cells (RBC), hemoglobin (Hb), packed cell volume (PCV), total platelet count (TPC), mean corpuscular volume (MCV), and mean corpuscular hemoglobin concentration (MCHC) using an automated blood analyzer (ABX Micros ESV60, Horiba, Kyoto, Japan).

Separation of peripheral blood mononuclear cells (PBMCs) and splenocytes

The pooled blood samples were used for isolation of PBMCs using Histopaque by density gradient centrifugation as described previously by Saminathan et al. [17]. Splenocytes were separated from the spleen of IFNAR blocked-infected, isotype-infected and non-infected control groups. The isolated PBMCs and splenocytes were mixed with stain buffer, cell numbers were counted by trypan blue dye exclusion method and the concentration was adjusted to 1×10^6/μL cells per sample.

Fluorescence-activated cell sorting (FACS)

The percentage of CD4$^+$ and CD8$^+$ T lymphocytes, and NK cells in PBMCs and splenocytes in the IFNAR blocked-infected, isotype-infected and non-infected control groups were estimated using mouse T lymphocyte subset cocktail monoclonal antibody with isotype control labeled with PE-CD4, FITC-CD8 and PE-Cy™7 CD3e, and PE-Cy™7 anti-mouse NK-1.1 by flow cytometric analysis as described previously by Saminathan et al. [17]. Ten thousand cells in each sample was counted by BD FACS Canto II Flow Cytometer using FL2 (CD4-PE) and FL1 (CD8-FITC), and 50,000 cells in each sample was counted using FL3 (NK-PE-Cy™7) band pass filters.

Preparation of spleen tissue homogenate

The spleen tissues (500 mg) were rinsed thoroughly in chilled PBS, minced into minute pieces (approx. 1 mm^3), and homogenized in 500 μL of PBS. The suspension was sonicated, freeze thawed repeatedly to break the cell membranes and the supernatant was stored at −80 °C.

Estimation of cytokines by c-ELISA

The cytokines namely, type I IFNs (IFN-α and IFN-β) and Th1 cell cytokine [interferon-gamma (IFN-γ)] were estimated from serum and spleen homogenate, and Th2 cell cytokine [interleukin-6 (IL-6)] and pro-inflammatory cytokines [tumor necrosis factor-α (TNF-α), interleukin-1β (IL-1β), and interleukin-12 (IL-12)] were estimated from spleen homogenate using the c-ELISA kit at different time intervals. The type I IFNs were estimated using mouse IFN-α (Cat. No: E03I0343) and mouse IFN-β (Cat. No: E03I0344) c-ELISA kits. Mouse IFN-γ (Cat. No: E03I0345), TNF-α (Cat. No: E03T0008), IL-1β (Cat. No: E03I0010), IL-6 (Cat. No: E03I0006), and IL-12 (Cat. No: E03I0033) cytokines were estimated using c-ELISA kit (BlueGene Biotech, Shanghai, China) according to the manufacturer's instructions. The intensity of the color was inversely proportional to the cytokine concentration. The standard curve was used to calculate the concentration in unknown samples. The sensitivity of this kit was 1.0 pg/mL.

Quantification of cytokines gene expression

The mRNA gene expression levels of different cytokines namely, IFN-α, IFN-β, IFN-γ, IL-6, TNF-α, IL-1β, IL-12, inducible nitric oxide synthase (iNOS), and FasL were estimated in the blood, draining LNs and spleen of IFNAR blocked-infected, non-infected and isotype-infected control groups at the specified time intervals by qRT-PCR using QuantiFast™ SYBR™ Green PCR Kit. The GAPDH was used as internal reference gene. The gene specific primer sequences of different cytokines are shown in Table 1.

The cDNA was synthesized from total RNA using RevertAid First Strand cDNA synthesis kit (Thermo Scientific, Carlsbad, CA, USA). The reverse transcription reaction was performed with 1 μL of random hexamer primers and approximately 500 ng of RNA template, and incubated at 65 °C for 5 min for denaturation. The reaction mixture was again incubated at 25 °C for 5 min followed by 42 °C for 60 min. The reaction was terminated by heating at 70 °C for 5 min. The qRT-PCR reactions were performed in 10 μL of reaction mixture in 0.2 mL clear PCR strips with flat optical caps. The amplification of each gene was performed using optimized thermal cyclic conditions, and Ct value, amplification plot and dissociation curve were stored for further analysis. Gene expressions were calculated by quantification of the cDNA with respect to the cDNA from uninfected mice as calibrator. All quantifications were normalized with respect to GAPDH (endogenous control). The relative values were expressed as $2^{-\Delta\Delta Ct}$, where ΔCt was the difference between Ct value of sample and GAPDH in the same

Table 1
Details of cytokine primers used in this study.

Gene	Primer sequence (5′–3′)	Annealing temperature (°C)	Product length (bp)	Reference
GAPDH	F: TGCACCACCAACTGCTTAG R: GGATGCAGGGATGATGTTC	56	120	McCarthy et al. [22]
IFN-α	F: AGGACAGGAAGGATTTTGGA R: GCTGCTGATGGAGGTCATT	62	200	McKimmie et al. [23]
IFN-β	F: CTGGAGCAGCTGAATGGAAAG R: CTTGAAGTCCGCCCTGTAGGT	62	200	Samuel and Diamond [24]
IFN-γ	F: GCTTTGCAGCTCTTCCTCATG R: CTTCCACATCTATGCCACTTGAG	61	101	Chen et al. [25]
TNF-α	F: CCACCACGCTCTTCTGTCTAC R: AGGGTCTGGGCCATAGAACT	56	102	Allam et al. [26]
IL-1β	F: AGTCTGCAGAGTTCCCCAAC R: ACCACTGTTGTTTCCCAGGA	60	80	Self designed
IL-6	F: GGAGTCACAGAAGGAGTGGC R: TGCCGAGTAGATCTCAAAGTGA	61	96	Li et al. [27]
IL-12p40	F: TTGCTGGTGTCTCCACTCATG R: GTCACAGGTGAGGTTCACTGTTTC	56	113	Chen et al. [25]
iNOS	F: TGCATGGACCAGTATAAGGCAAGC R: GCTTCTGGTCGATGTCATGAGCAA	58	223	Doi et al. [28]
FasL	F: GAGAATTGCTGAAGACATGACAATCC R: ATGGCTGGAACTGAGGTAGTTTTCAC	58	320	Ubol et al. [29]

sample. The $\Delta\Delta Ct$ was the difference between ΔCt value of sample and the calibrator (uninfected mice).

Analysis of early apoptotic cells in PBMCs

The PBMCs from IFNAR blocked-infected, isotype-infected and non-infected control groups were analyzed for apoptotic cells by flow cytometry using TACS™ Annexin V-FITC Apoptosis Detection Kit as described previously by Saminathan et al. [17]. Ten thousand cells were counted by BD FACS Canto II Flow Cytometer using FL1 (Annexin V-FITC-early apoptotic) and FL3 (PI-late apoptotic or necrotic) band pass filters. The results were plotted as percentage of annexin-V$^+$PI$^-$ cells.

Detection of apoptotic cells in tissues

The apoptotic cells were detected in formalin fixed tissue sections using *In Situ* Cell Death Detection Kit. The stained slides were viewed under a fluorescence microscope.

Serum biochemistry

At each interval, serum samples were analyzed for biochemical parameters namely, serum glutamic oxaloacetic transaminase (SGOT), serum glutamic-pyruvic transaminase (SGPT), alkaline phosphatase (ALP), and creatine kinase (CK) using kits of Coral Clinical Systems as per the manufacturer's protocol. The OD values were measured in the MultiskanGo spectrophotometer (Thermo Scientific, Carlsbad, California, USA).

Statistical analysis

The data were analyzed using GraphPad Prism, Version 5.0. The effects of BTV-1 in infected and non-infected control groups were analyzed using two-way ANOVA with Bonferroni post-test. The means of the control and infected groups at specific time intervals were expressed as mean ± standard error of the mean (SEM) and differences were considered significant at $P < 0.05$.

Results

Clinical signs

The IFNAR blocked-infected mice showed clinical signs of ruffled hair coat, slightly reduced activity, and mild apathy at 1 dpi. Marked apathy, weight loss, sluggish movement, huddling tendency, hunched posture, conjunctivitis, and porphyrin staining became more apparent from 2 dpi onward. Respiratory signs such as dyspnea, ocular and nasal discharges, snuffling, and chattering started from 5 dpi onward. Mortality started at 6 dpi, severe disease progression led to high mortality at 7–9 dpi, and the details of mortality are mentioned in Fig. 1. Isotype-infected control and non-infected control groups did not show any clinical signs or mortality throughout the experimental period. The evaluation and scoring of the individual clinical signs in the IFNAR blocked-infected, isotype-infected and non-infected control groups were mentioned in Table 2.

Gross and histopathological lesions

The axillary (Fig. 2a) and inguinal (Fig. 2d) LNs from non-infected control animals did not show any gross and histopathological lesions (Fig. 3a). The axillary (Fig. 2b) and inguinal (Fig. 2e) LNs from isotype-infected control animals showed mild enlargement. Markedly enlarged, edematous, congested, and hem-
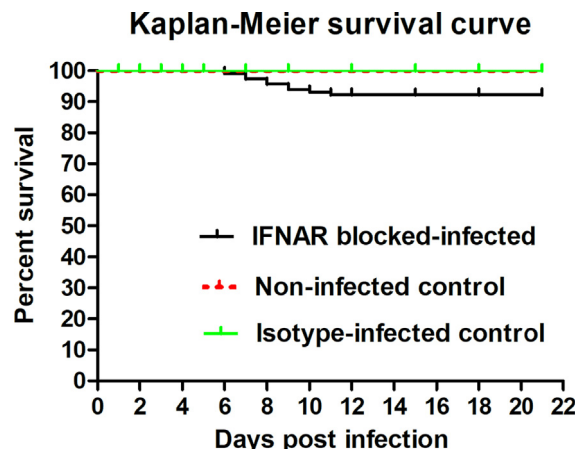

Fig. 1. Kaplan–Meier survival curve. Wild-type adult mice (n = 30) were injected intraperitoneally (I/P) with 1.5 mg/mouse of anti-mouse IFN-α/β receptor monoclonal antibody (Clone: MAR1-5A3) one day prior to BTV infection and 0.5 mg/mouse one day after BTV infection. On day 0, mouse were inoculated intravenously (I/V) with BTV-1 and acted as IFNAR blocked-infected group. Mice (n = 27) were inoculated I/V with culture medium without BTV and I/P with MAR1-5A3 antibody as described above and acted as non-infected control group. Mice (n = 27) were inoculated I/P with the same dose of mouse IgG isotype one day prior to and one day after BTV infection and acted as isotype-infected control group. Mortality was recorded daily.

orrhagic axillary (Fig. 2c) and inguinal (Fig. 2f) LNs were observed from 3 dpi onward.

Histopathologically, congestion and hemorrhages in subcapsular sinus of LNs were observed at 3 dpi onward. Marked lymphoid depletion with "starry-sky pattern" characterized by shrinkage of cells and condensation of nucleus and chromatin suggestive of apoptosis were observed in the cortex of LNs at 5 dpi onward (Fig. 3b). Necrosis of lymphoid follicles was observed in LNs at 7–9 dpi (Fig. 3c). Reactive lymphadenitis with marked infiltration of macrophages, plasma cells and dendritic cells (DCs) in the paracortical region and medullary sinuses were observed at 9–15 dpi. Hyperplasia of cortical lymphoid follicles with germinal center formation was noticed at 12–15 dpi (Fig. 3d).

Grossly, spleen became congested at 3–5 dpi and shrunken at 7–9 dpi (Fig. 4a). Markedly enlarged and edematous spleen was observed at 12–15 dpi (Fig. 4b). Spleen from isotype-infected control animals showed mild enlargement and non-infected control animals did not show any gross and histopathological (Fig. 4a–c) lesions. Histopathologically, marked lymphoid depletion was observed in white pulp at 7 dpi onward. The "Starry-sky pattern" due to apoptosis of lymphocytes in white pulp areas (Fig. 4d) and deposition of golden-brown hemosiderin pigments in red pulp areas were observed at 5–9 dpi (Fig. 4e). Neutrophilic infiltration in subcapsular sinuses, and white and red pulp areas were observed at 7 dpi onward (Fig. 4e). Germinal center formation and hyperplasia of white pulp with increased number and size of follicles were observed at 12–15 dpi (Fig. 4f).

Grossly, thymus became congested and edematous at 3–5 dpi, hemorrhagic at 5–7 dpi, and markedly enlarged at 9–15 dpi. Thymus from isotype-infected and non-infected control animals did not show any gross and histopathological (Supplementary Fig. 2a) changes. Histopathologically, thymus showed congestion with swollen endothelial cells at 3–5 dpi, and hemorrhages in the cortico-medullary junction were observed at 5–7 dpi (Supplementary Fig. 2b). Necrosis of thymocytes in the cortical area was observed at 7–9 dpi (Supplementary Fig. 2c). Thymic hyperplasia with reduced medullary areas due to proliferation of cortical epithelial cells into medullary areas was observed at 9 to 15 dpi (Supplementary Fig. 2d).

Table 2
Evaluation and scoring of the individual clinical signs in mice after challenge with BTV-1.

IFNAR blocked-infected group			Isotype-infected control group			Non-infected control group		
Mouse No.	Clinical score on day of sacrifice	Day of sacrifice/mortality	Mouse No.	Clinical score on day of sacrifice	Day of sacrifice/mortality	Mouse No.	Clinical score on day of sacrifice	Day of sacrifice/mortality
1.1	4	Sacrificed on 2 dpi	2.1	0	Sacrificed on 2 dpi	3.1	0	Sacrificed on 2 dpi
1.2	8	Sacrificed on 2 dpi	2.2	0	Sacrificed on 2 dpi	3.2	0	Sacrificed on 2 dpi
1.3	5	Sacrificed on 2 dpi	2.3	0	Sacrificed on 2 dpi	3.3	0	Sacrificed on 2 dpi
1.4	9	Sacrificed on 3 dpi	2.4	0	Sacrificed on 3 dpi	3.4	0	Sacrificed on 3 dpi
1.5	7	Sacrificed on 3 dpi	2.5	0	Sacrificed on 3 dpi	3.5	0	Sacrificed on 3 dpi
1.6	8	Sacrificed on 3 dpi	2.6	0	Sacrificed on 3 dpi	3.6	0	Sacrificed on 3 dpi
1.7	10	Sacrificed on 5 dpi	2.7	0	Sacrificed on 5 dpi	3.7	0	Sacrificed on 5 dpi
1.8	14	Sacrificed on 5 dpi	2.8	0	Sacrificed on 5 dpi	3.8	0	Sacrificed on 5 dpi
1.9	12	Sacrificed on 5 dpi	2.9	0	Sacrificed on 5 dpi	3.9	0	Sacrificed on 5 dpi
1.10	18	Died on 6 dpi	2.10	0	Sacrificed on 7 dpi	3.10	0	Sacrificed on 7 dpi
1.11	16	Died on 7 dpi	2.11	0	Sacrificed on 7 dpi	3.11	0	Sacrificed on 7 dpi
1.12	19	Died on 7 dpi	2.12	0	Sacrificed on 7 dpi	3.12	0	Sacrificed on 7 dpi
1.13	17	Died on 8 dpi	2.13	0	Sacrificed on 9 dpi	3.13	0	Sacrificed on 9 dpi
1.14	18	Died on 9 dpi	2.14	0	Sacrificed on 9 dpi	3.14	0	Sacrificed on 9 dpi
1.15	19	Died on 9 dpi	2.15	0	Sacrificed on 9 dpi	3.15	0	Sacrificed on 9 dpi
1.16	19	Died on 9 dpi	2.16	0	Sacrificed on 12 dpi	3.16	0	Sacrificed on 12 dpi
1.17	17	Died on 10 dpi	2.17	0	Sacrificed on 12 dpi	3.17	0	Sacrificed on 12 dpi
1.18	16	Died on 11 dpi	2.18	0	Sacrificed on 12 dpi	3.18	0	Sacrificed on 12 dpi
1.19	16	Sacrificed on 12 dpi	2.19	0	Sacrificed on 15 dpi	3.19	0	Sacrificed on 15 dpi
1.20	15	Sacrificed on 12 dpi	2.20	0	Sacrificed on 15 dpi	3.20	0	Sacrificed on 15 dpi
1.21	12	Sacrificed on 12 dpi	2.21	0	Sacrificed on 15 dpi	3.21	0	Sacrificed on 15 dpi
1.22	11	Sacrificed on 15 dpi	2.22	0	Sacrificed on 18 dpi	3.22	0	Sacrificed on 18 dpi
1.23	9	Sacrificed on 15 dpi	2.23	0	Sacrificed on 18 dpi	3.23	0	Sacrificed on 18 dpi
1.24	9	Sacrificed on 15 dpi	2.24	0	Sacrificed on 18 dpi	3.24	0	Sacrificed on 18 dpi
1.25	8	Sacrificed on 18 dpi	2.25	0	Sacrificed on 21 dpi	3.25	0	Sacrificed on 21 dpi
1.26	6	Sacrificed on 18 dpi	2.26	0	Sacrificed on 21 dpi	3.26	0	Sacrificed on 21 dpi
1.27	7	Sacrificed on 18 dpi	2.27	0	Sacrificed on 21 dpi	3.27	0	Sacrificed on 21 dpi
1.28	6	Sacrificed on 21 dpi						
1.29	4	Sacrificed on 21 dpi						
1.30	5	Sacrificed on 21 dpi						

Each mouse from different groups was monitored for individual clinical signs that are scored by following the modified method of Jabbar et al. (2013) and Marin-Lopez et al. (2018). The following individual clinical signs were monitored: Activity: normal 0, slightly reduced 1, reduced 2 and severely reduced 3; Apathy: absent 0, mild 1 and marked 2; Hunched posture/huddling tendency: absent 0, mild 1 and marked 2; Ruffled or rough hair coat: absent 0, mild 1 and marked 2; Alopecia: absent 0, mild 1 and marked 2; Ocular and nasal discharges: absent 0, mild 1 and marked 2; Dyspnea/snuffling/chattering: absent 0, mild 1 and marked 2; Swelling around the eyes: absent 0, mild 1 and marked 2; and Weight loss: absent 0, mild 1 and marked 2. The final clinical score for each mouse was the sum of all the scores of clinical signs. The minimum score was 0 for healthy and 1 to 19 depending upon the severity of clinical signs.

Grossly, tracheal mucosa was edematous, congested and hemorrhagic at 5 to 9 dpi. Histopathologically, mild hemorrhagic tracheitis was observed at 3–5 dpi, and the lesions became severe at 7–9 dpi characterized by hemorrhagic exudate containing RBCs, sloughed tracheal epithelial cells, lymphocytes and macrophages in the tracheal lumen (Fig. 3e), submucosal hemorrhages, and edema. Grossly, lungs showed vascular lesions such as congestion, severe edema, and hemorrhages at 5 dpi onward. Lungs were enlarged, emphysematous and showed pneumonic lesions such as consolidation in right cranial, caudal and entire left lobes at 7 dpi onward. Lung lesions became complicated due to BTV-induced immunosuppression resulted in secondary bacterial infection at 7 dpi onward, evidenced by marked neutrophil infiltration in alveoli, bronchi and bronchioles (Fig. 3h) at 12–15 dpi. The lungs from isotype-infected and non-infected control animals did not show any gross and histopathological (Fig. 3f) changes. Histopathologically, IFNAR blocked-infected lungs showed mild congestion at 2 dpi and moderate congestion with mild thickening of inter-alveolar septa at 3 dpi. Severe congestion of inter-alveolar capillaries, swollen endothelial cells, severe edema with eosinophilic exudates and hemorrhages in the alveolar lumen and around the blood vessels, and hyalinization of tunica media of pulmonary artery were found at 5–9 dpi. The lesions progressed to severe necro-hemorrhagic lesions at 7–9 dpi. Interstitial pneumonia characterized by severe diffusely thickened inter-alveolar septa due to proliferation of alveolar epithelial cells and infiltration of mononuclear cells such as lymphocytes and macrophages was observed at 5 dpi onward (Fig. 3g).

Grossly, congestion, edema and petechial hemorrhages were found in the liver, epicardial surface and kidneys at 5 dpi onward. Congestion of meningeal blood vessels and edema of brain parenchyma was observed at 7 dpi onward. Histopathologically, congestion and hemorrhages in the epicardium and myocardium at 5 dpi, loss of striations of cardiac muscle fibers and infiltration of
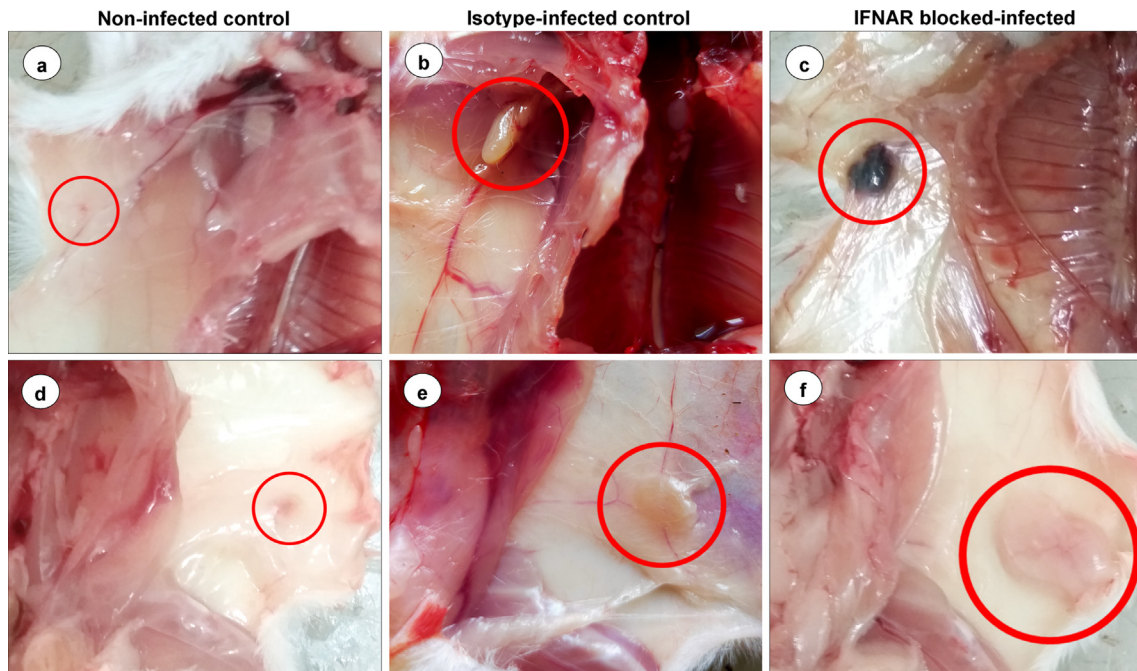
Fig. 2. (a) Non-infected healthy control mice (n = 27) showed indistinct axillary lymph node in subcutaneous fat. (b) Axillary LNs from isotype-infected control mice (n = 3) showed mild enlargement at 3 dpi. (c) IFNAR blocked-infected mice (n = 3) showed markedly enlarged, edematous and congested axillary lymph node at 3 dpi. (d) Non-infected control mice (n = 27) showed indistinct inguinal lymph node in subcutaneous fat. e. Inguinal LNs from isotype-infected control animals (n = 3) showed mild enlargement at 3 dpi. (f) IFNAR blocked-infected mice (n = 3) showed markedly enlarged and edematous inguinal lymph node at 3 dpi.

mononuclear cells in the myocardium were observed at 7–9 dpi (Supplementary Fig. 3a, b). The liver showed sinusoidal congestion and hemorrhages at 5–7 dpi (Supplementary Fig. 3e), perivascular edema, necrosis, and infiltration of inflammatory cells in the muscular wall of the hepatic artery and swollen endothelial cells were observed at 9–12 dpi. The brain showed moderate congestion in meninges and brain parenchyma at 7 dpi, which later on progressed to severe meningitis, prominent endothelial swelling and peri-vascular cuffing at 7–9 dpi (Supplementary Fig. 3g). The cortex and medulla of kidneys showed congestion and focal hemorrhagic areas at 5–7 dpi and infiltration of inflammatory cells were observed at 9–12 dpi.

Gross and histopathological lesions were not observed in the adrenals, stomach, intestine, pancreas, uterus, and ovary of IFNAR blocked-infected, isotype-infected and non-infected control groups throughout the experiment.

Quantification of BTV nucleic acid using qRT-PCR

Bluetongue viral RNA was quantified in blood and various tissues from IFNAR blocked-infected and isotype-infected control mice using qRT-PCR (Table 3). The BTV was detected in the blood and spleen from 2 to 21 dpi and the highest copy number was detected at 7 and 9 dpi, respectively. In isotype-infected control group, BTV nucleic acid was detected from LNs on 2 dpi only, and in blood and spleen up to 3 dpi only, thereafter no viral RNA was detected any of the organs. The non-infected control mice remained negative throughout the experiment.

Localization of BTV antigen in tissues

Bluetongue viral antigen was localized in the draining LNs (axillary and inguinal LNs) (Fig. 5c), spleen (Fig. 5d), thymus, trachea (Fig. 3e), lungs (Figs. 3h, 5e,f), heart (Supplementary Fig. 3c), liver (Supplementary Fig. 3f), and brain (Supplementary Fig. 3h) of IFNAR blocked-infected mice. Positive signals were detected pri-

marily in the medulla rather than cortex of LNs at 3 dpi onward (Fig. 5c). In the LNs and spleen, BTV antigen was detected in the endothelial cells, macrophages, lymphocytes, and stellate cells.

In lungs, BTV antigen was localized in the alveolar macrophages, endothelial cells (Fig. 5e, f), bronchial and bronchiolar epithelium (Fig. 3h), and peribronchial lymphocytes. At 5 dpi and onward, tracheal epithelium (Fig. 3e), endocardial valve (Supplementary Fig. 3c), myocardium, endothelial cells lining the capillaries in the liver and brain (Supplementary Fig. 3f), and neurons and glial cells (Supplementary Fig. 3h) showed presence of BTV antigen. In isotype-infected control group, few macrophages and lymphocytes showed positive immunolabelling of BTV antigen in LNs at 2 dpi and in spleen at 3 dpi only (Fig. 5b), and thereafter no antigen was demonstrated in any of the organs. Non-infected control animals did not show positive signals in any of these target organs (Fig. 5a, Supplementary Fig. 3d) throughout the experiment.

Humoral immune response

The IFNAR blocked-infected animals were negative for antibodies against the group specific core protein VP7 up to 5 dpi, and at 7 dpi onward showed positivity for BTV antibodies (Supplementary Fig. 4). The antibody levels peaked at 15 dpi (80.60%), and thereafter started to decrease. The isotype-infected control mice remained negative for BTV antibodies up to 9 dpi and at 12 dpi onward showed positive for BTV antibodies; however, the levels were low. The non-infected control animals remained negative for BTV antibodies throughout the experimental period (Supplementary Fig. 4).

Assessment of cell mediated immunity

TLC and DLC

The IFNAR blocked-infected group showed decreased counts of TLC and lymphocyte (P < 0.01) up to 7 dpi compared to the non-infected control mice. Subsequently, the counts of TLC and lym-
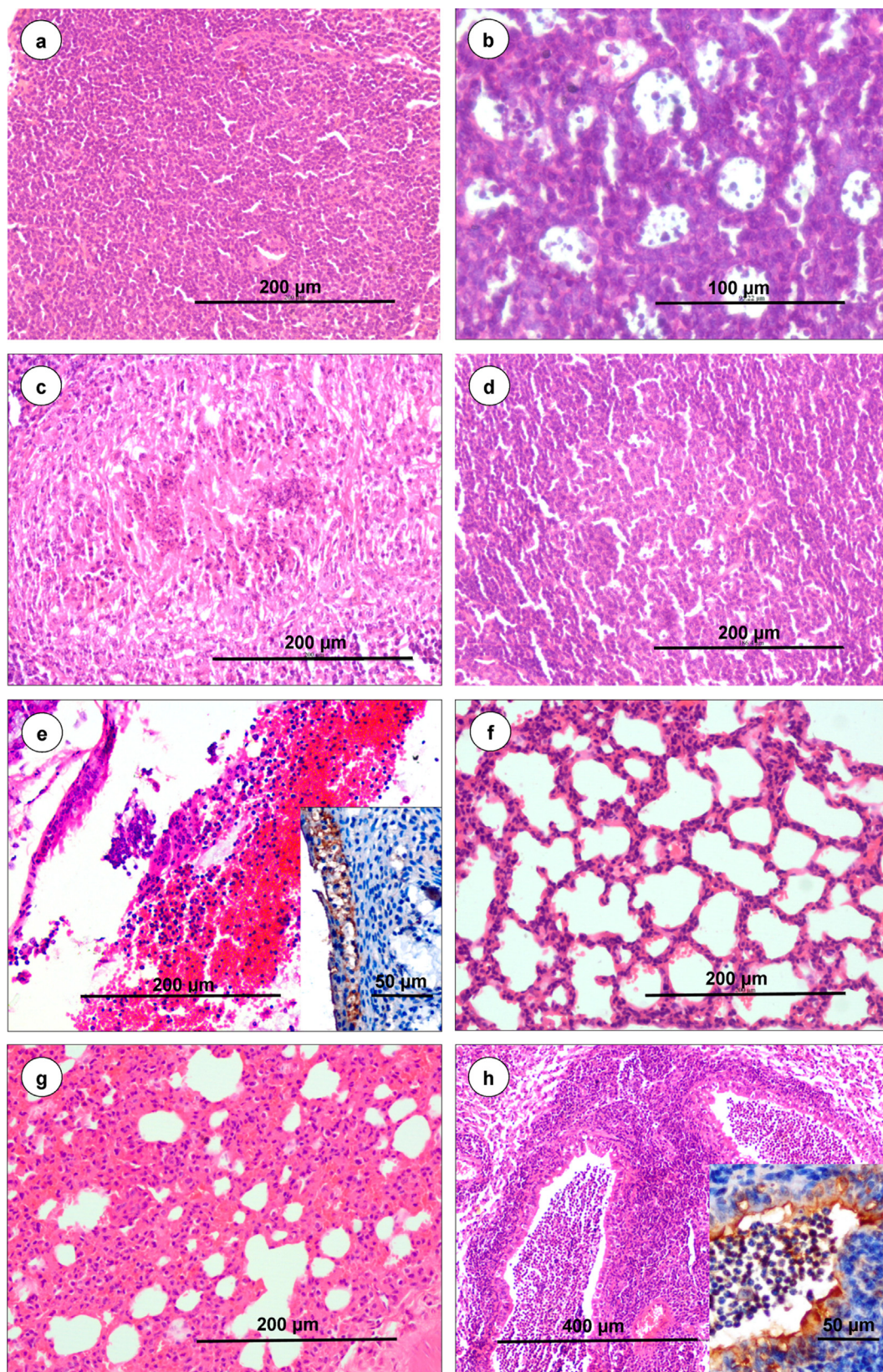
Fig. 3. Representative histopathology images in isotype-infected control (a and f) and IFNAR blocked-infected (b–e, g and f) groups. (a) Isotype-infected control (n = 27) lymph node showed normal cortex and medulla. H&E, scale bar 200 μm. (b) Starry-sky pattern due to apoptosis of lymphocytes in lymphoid follicle at 7 dpi (n = 3). H&E, scale bar 100 μm. (c) Necrosis and lymphocytolysis in cortex of lymph node at 9 dpi (n = 3). H&E, scale bar 200 μm. (d) Germinal centre formation with hyperplasia of lymphoid follicles at 15 dpi (n = 3). H&E, scale bar 200 μm. e. Hemorrhagic exudate containing RBCs, sloughed tracheal epithelial cells and lymphocytes in the tracheal lumen at 7 dpi (n = 3). H&E, scale bar 200 μm. Inset showed positive immunolabelling of BTV-1 antigen in tracheal epithelium. IP-DAB-MH, scale bar 50 μm. (f) Isotype-infected control lungs showed normal histology (n = 27). H&E, scale bar 200 μm. (g) Alveolar septa are diffusely thickened with proliferation of alveolar epithelial cells, infiltration of mononuclear cells and marked congestion in inter-alveolar capillaries at 7 dpi (n = 3). H&E, scale bar 200 μm. (h) Bronchopneumonia: Marked neutrophilic infiltration in bronchioles at 12 dpi (n = 3). H&E, scale bar 200 μm. Inset showed positive immunolabelling of BTV antigen in bronchial epithelium and exudates. IP-DAB-MH, scale bar 50 μm.
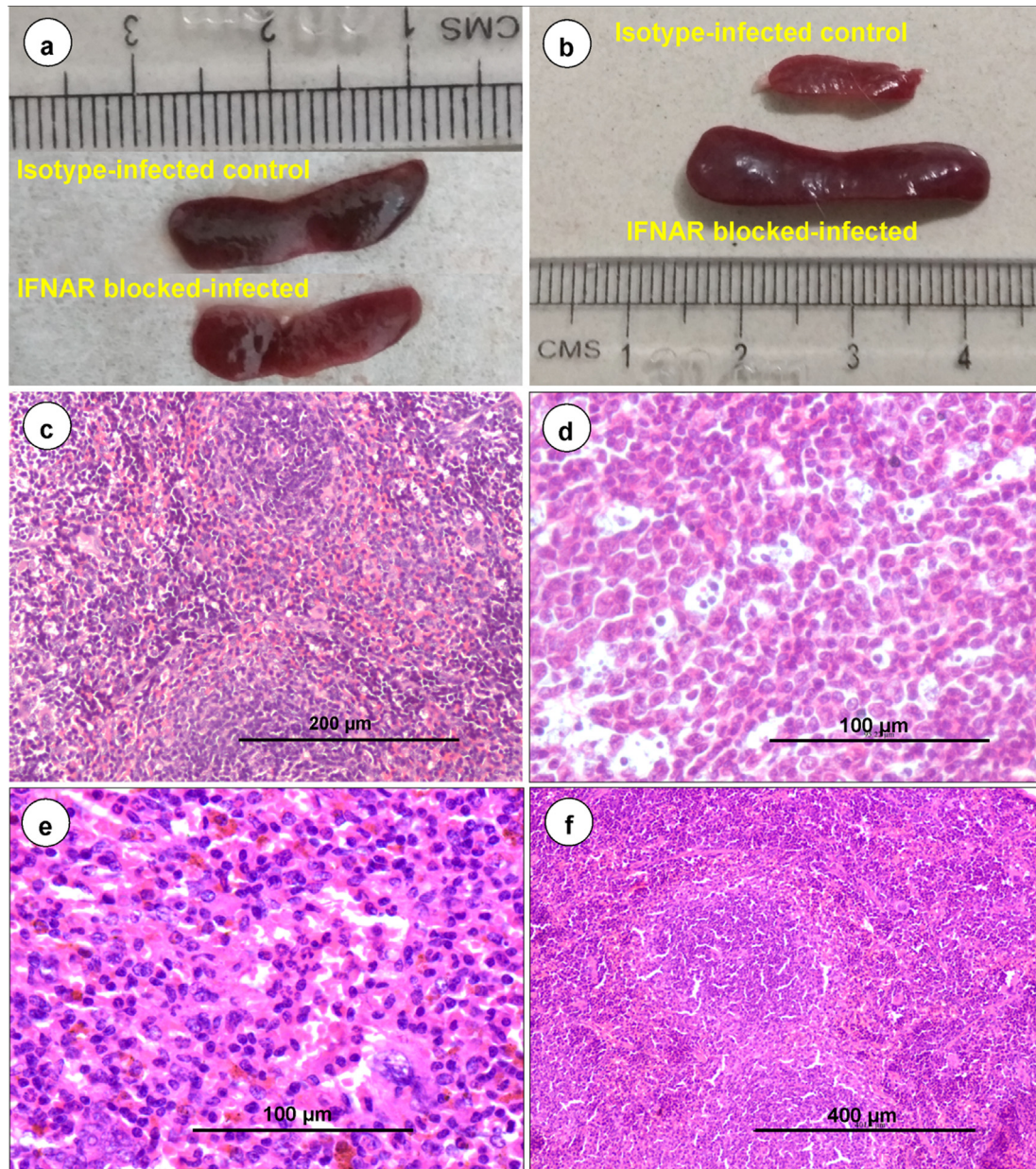
Fig. 4. (a) IFNAR blocked-infected spleen was found shrunken at 7 dpi (n = 3). (b) Spleen showed marked enlargement and widespread edema at 15 dpi (n = 3). (c) Isotype-infected control spleen showed normal white and red pulp areas (n = 27). H&E, scale bar 200 μm. (d) Starry-sky pattern due to apoptosis of lymphocytes in white pulp at 7 dpi (n = 3). H&E, scale bar 100 μm. e. Spleen showed lymphoid depletion, golden brown hemosiderin pigments and neutrophilic infiltration at 7 dpi (n = 3). H&E, scale bar 100 μm. (f) IFNAR blocked-infected spleen showed hyperplasia of white pulp at 15 dpi (n = 3). H&E, scale bar 400 μm.

phocyte were increased at 15 dpi compared to isotype-infected and non-infected controls (Supplementary Fig. S5a, b). The neutrophil count in the IFNAR blocked-infected group increased significantly at 7 (P < 0.01) and 9 (P < 0.05) dpi than isotype-infected control and non-infected control groups (Supplementary Fig. 5c). Monocyte count in the infected group decreased non-significantly at 7 dpi and increased thereafter. The basophil and eosinophil counts did not reveal any significant changes in the IFNAR blocked-infected mice compared to the isotype-infected and non-infected controls.

Kinetics of CD4$^+$ and CD8$^+$ T cells

The T lymphocyte subsets in PBMCs and spleen from IFNAR blocked-infected group showed significant (P < 0.05) changes at various time points (Fig. 6a–d). The CD4$^+$ and CD8$^+$ T cells in PBMCs showed significant decrease at 9 and 7 dpi, respectively, and there-

after, CD8$^+$ T cells only increased significantly (P < 0.001) from 12 to 18 dpi compared to isotype-infected and non-infected control groups (Fig. 6e, f). In spleen, significant (P < 0.01) decrease of CD4$^+$ and CD8$^+$ T cells were recorded at 7 dpi (Fig. 6e, f). Subsequently, CD8$^+$ T cells in spleen started to increase from 12 to 18 dpi and showed a significant (P < 0.001) increase at 15 dpi than isotype-infected and non-infected control groups (Fig. 6f). In isotype-infected and non-infected control groups, CD4$^+$ and CD8$^+$ T cells did not show any significant changes (Fig. 6e, f).

Kinetics of CD4$^+$ and CD8$^+$ T cells ratio

In PBMCs and spleen, CD4$^+$ and CD8$^+$ T cells ratio increased significantly at 7 dpi, subsequently, the levels decreased significantly in PBMCs at 15 dpi and in spleen at 12 and 15 dpi in the IFNAR blocked-infected group than isotype-infected and non-infected

Table 3
Quantification of BTV by qRT-PCR from blood and tissue samples at different time points.

Tissue names	Groups	Days post infection (dpi)								
		2	3	5	7	9	12	15	18	21
Blood	IFNAR blocked-infected	2.67 ± 0.28	4.13 ± 0.17	5.08 ± 0.11	6.43 ± 0.19	5.88 ± 0.15	5.16 ± 0.26	4.45 ± 0.15	3.18 ± 0.18	2.56 ± 0.09
	Isotype-infected control	0.91 ± 0.27	0.52 ± 0.17	ND	ND	ND	ND	ND	ND	ND
Axillary lymph node	IFNAR blocked-infected	1.76 ± 0.16	3.23 ± 0.15	5.36 ± 0.25	4.87 ± 0.18	4.06 ± 0.28	2.44 ± 0.19	1.16 ± 0.09	ND	ND
	Isotype-infected control	0.42 ± 0.35	ND	ND	ND	ND	ND	ND	ND	ND
Inguinal lymph node	IFNAR blocked-infected	2.33 ± 0.18	3.89 ± 0.15	5.76 ± 0.22	5.18 ± 0.21	4.63 ± 0.19	2.56 ± 0.11	1.23 ± 0.14	ND	ND
	Isotype-infected control	0.51 ± 0.24	ND	ND	ND	ND	ND	ND	ND	ND
Spleen	IFNAR blocked-infected	1.26 ± 0.09	2.63 ± 0.11	3.73 ± 0.16	5.36 ± 0.2	6.22 ± 0.19	5.06 ± 0.11	4.38 ± 0.17	3.26 ± 0.12	2.58 ± 0.11
	Isotype-infected control	0.75 ± 0.27	0.49 ± 0.17	ND	ND	ND	ND	ND	ND	ND
Lungs	IFNAR blocked-infected	ND	0.76 ± 0.07	2.23 ± 0.1	4.78 ± 0.36	5.23 ± 0.28	4.73 ± 0.24	3.46 ± 0.21	1.63 ± 0.18	1.29 ± 0.13
	Isotype-infected control	ND	0.41 ± 0.07	ND	ND	ND	ND	ND	ND	ND
Thymus	IFNAR blocked-infected	1.79 ± 0.08	2.25 ± 0.17	3.76 ± 0.12	4.66 ± 0.14	4.38 ± 0.28	3.56 ± 0.39	2.85 ± 0.18	1.85 ± 0.25	ND
	Isotype-infected control	0.66 ± 0.19	0.39 ± 0.28	ND	ND	ND	ND	ND	ND	ND
Heart	IFNAR blocked-infected	ND	1.86 ± 0.06	3.48 ± 0.16	4.33 ± 0.18	4.28 ± 0.19	3.68 ± 0.13	2.86 ± 0.27	1.68 ± 0.2	ND
	Isotype-infected control	ND	0.38 ± 0.26	ND	ND	ND	ND	ND	ND	ND
Brain	IFNAR blocked-infected	ND	ND	1.86 ± 0.19	2.36 ± 0.16	3.26 ± 0.28	2.43 ± 0.23	1.09 ± 0.11	ND	ND
	Isotype-infected control	ND	ND	ND	ND	ND	ND	ND	ND	ND
Uterus	IFNAR blocked-infected	ND	ND	1.13 ± 0.15	1.47 ± 0.18	1.25 ± 0.16	1.18 ± 0.15	0.88 ± 0.18	ND	ND
	Isotype-infected control	ND	ND	ND	ND	ND	ND	ND	ND	ND
Ovaries	IFNAR blocked-infected	ND	ND	0.96 ± 0.15	1.14 ± 0.26	1.18 ± 0.19	1.02 ± 0.17	0.75 ± 0.09	ND	ND
	Isotype-infected control	ND	ND	ND	ND	ND	ND	ND	ND	ND

ND: Not detected.
Virus load in blood is given as $\log_{10}$ copies of viral RNA ml^{-1} of samples and virus load in tissues is given as $\log_{10}$ copies of viral RNA g^{-1} tissue. Results are presented as mean ± SEM at each time point.

control groups. The isotype-infected and non-infected control groups did not show any significant changes (Fig. 6g).

Kinetics of NK cells in PBMCs and spleen

Natural killer cells in PBMCs and spleen from IFNAR blocked-infected group showed non-significant changes at the specified time points (Fig. 6h). In PBMCs and spleen, the population of NK cells increased non-significantly at 2 dpi and subsequently, the levels became low at 7 dpi. Thereafter, the levels started to increase, and a non-significant increase was noticed at 15 dpi in PBMCs and spleen of IFNAR blocked-infected group than isotype-infected and non-infected control groups. No significant changes were noticed in NK cells in PBMCs and spleen of isotype-infected and non-infected control groups (Fig. 6h).

Estimation of cytokines by c-ELISA

The type I IFNs levels of the IFNAR blocked-infected group in serum and spleen homogenates were not detectable up to 3 dpi and levels were very minimal at 5 dpi. The type I IFNs levels were increased at 15 dpi in serum and spleen homogenate when compared to isotype-infected and non-infected control groups. However, the levels became minimal at 21 dpi as that of isotype-infected and non-infected control groups (Supplementary Fig. 6a, b). In isotype-infected control group, IFN-α level was more at 2 dpi in serum (5250 pg/mL) and spleen (8750 pg/mL), and at 3 dpi in serum (750 pg/mL) and spleen (1500 pg/mL), thereafter the levels were minimal as that of non-infected control group throughout the experiment. The IFN-β level was more at 2 dpi in serum (1500 pg/mL) and spleen (2750 pg/mL), and at 3 dpi in

serum (500 pg/mL) and spleen (500 pg/mL), thereafter the levels were minimal as that of non-infected control group throughout the experiment. The IFN-γ displayed a brief significant increase at 2 dpi and low levels were observed from 3 to 9 dpi in IFNAR blocked-infected group. However, the levels started to increase from 9 to 15 dpi, with a peak increase at 15 dpi, and thereafter started to decrease up to 21 dpi in the IFNAR blocked-infected group than the isotype-infected and non-infected control groups (Supplementary Fig. 6c).

The IL-6 and IL-12 showed no significant changes up to 5 dpi and significantly increased levels were noticed from 7 to 12 dpi, with a significant peak increase at 12 dpi and levels declined after 12 dpi, became minimal by 21 dpi in IFNAR blocked-infected group (Supplementary Fig. 6d, e). The concentration of TNF-α in spleen homogenates increased significantly from 5 to 12 dpi, with a significant peak increase at 12 dpi in the IFNAR blocked-infected group than isotype-infected and non-infected control groups (Supplementary Fig. 6f). The IL-1β did not show significant changes up to 5 dpi compared to isotype-infected and non-infected control groups. From 7 to 15 dpi, the levels showed significant changes with a peak increase at 12 dpi (Supplementary Fig. 6f). The IFN-γ, IL-6, IL-12, TNF-α and IL-1β from isotype-infected and non-infected control groups did not show any significant changes throughout the experiment (Supplementary Fig. 6a–f).

Quantification of cytokine gene expression by qRT-PCR

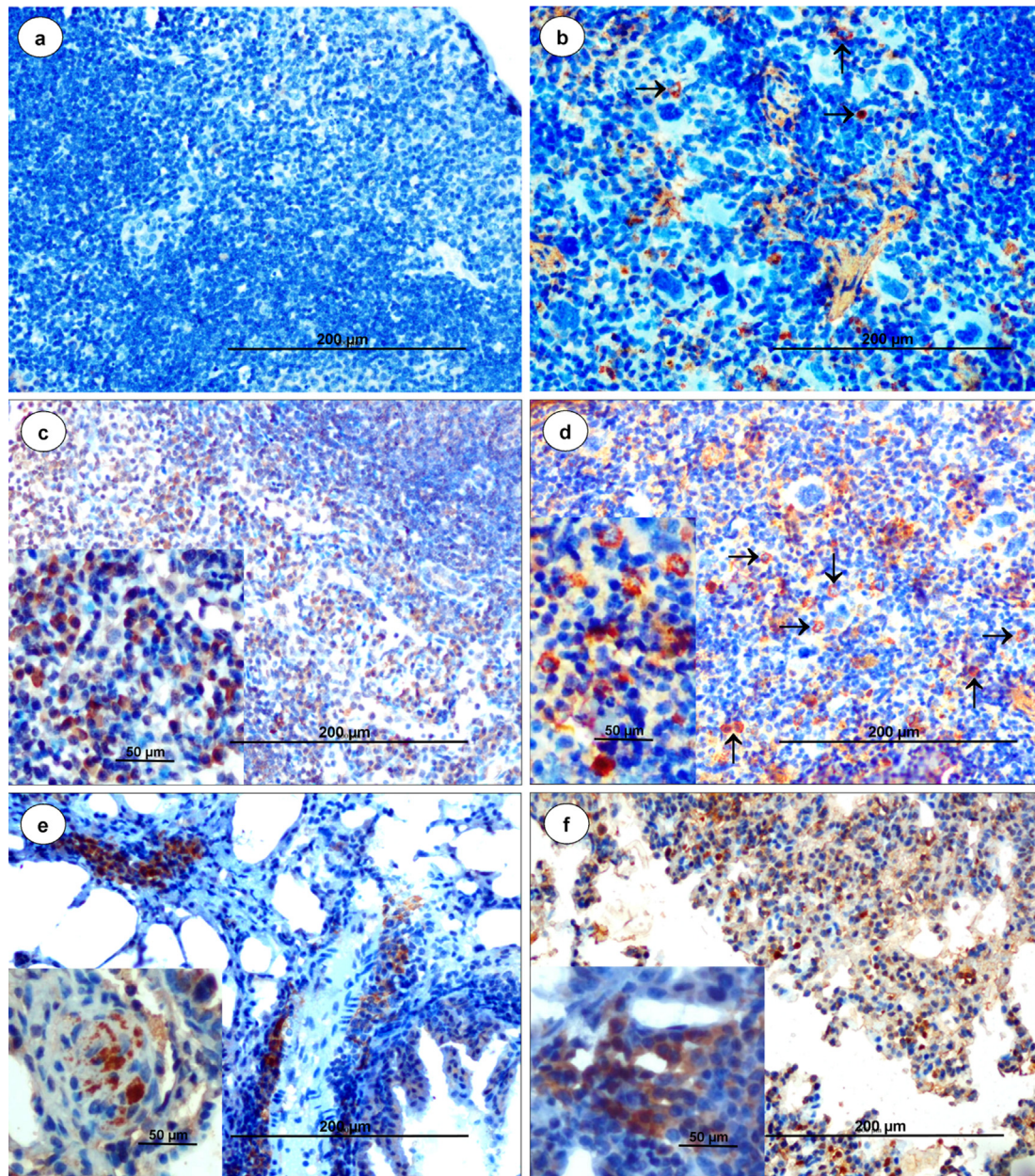The mRNA gene expression levels of IFN-α and IFN-β were downregulated in blood, draining LNs and spleen at 2–5 dpi in

Fig. 5. (a) Spleen from non-infected control animal showed no positive immunoreaction for BTV antigen (n = 27). IP-DAB-MH, scale bar 200 μm. (b) Spleen from isotype-infected control animal showed positive immunolabelling of BTV antigen in few macrophages and lymphocytes at 3 dpi (n = 3). IP-DAB-MH, scale bar 200 μm. (c) Lymph node from IFNAR blocked-infected animal showed strong immunolabelling of BTV antigen in macrophages, lymphocytes and stellate cells in medulla at 7 dpi (n = 3). IP-DAB-MH, scale bar 200 μm. Inset, IP-DAB-MH, scale bar 50 μm. (d) Spleen from IFNAR blocked-infected animal showed strong immunolabelling of BTV antigen in lymphocytes and histiocytes (arrow) at 9 dpi (n = 3). IP-DAB-MH, scale bar 200 μm. Inset, IP-DAB-MH, scale bar 50 μm. (e and f) Lungs from IFNAR blocked-infected animal showed strong immunolabelling of BTV antigen in alveolar macrophages, lymphocytes and endothelial cells at 9 dpi (n = 3). IP-DAB-MH, scale bar 200 μm. Inset, IP-DAB-MH, scale bar 50 μm.

the IFNAR blocked-infected group. At 7 dpi, IFN-α and IFN-β expression levels were low and at 12 dpi their expression levels were increased and at 21 dpi expression became low in IFNAR blocked-infected group (Fig. 7a, b). In isotype-infected control group, IFN-α and IFN-β expressions were increased at 2 dpi in blood (fold change 51.36 and 40.36, respectively), draining LNs (fold change 55.25 and 38.76, respectively) and spleen (fold change 102.9 and 42.91, respectively), and at 3 dpi in blood (fold change 10.15 and 8.04, respectively), draining LNs (fold change 13.62 and 7.24, respectively) and spleen (fold change 32.38 and 9.12, respectively); however, thereafter the expressions levels were minimal throughout the experiment (Fig. 7a, b).

The expressions of IFN-γ briefly increased at 2 and 3 dpi, and decreased from 5 to 7 dpi in IFNAR blocked-infected and isotype-infected control groups (Fig. 7c). However, the expression levels were increased from 12 to 15 dpi and then became low at 21 dpi in IFNAR blocked-infected group (Fig. 7c). The expressions of pro-inflammatory cytokines (TNF-α, IL-1β, and IL-12) were variable between the time points in the IFNAR blocked-infected group (Fig. 7d-f). The expressions of TNF-α were low from 2 and 3 dpi, moderate at 5 and 7 dpi, and high at 12 dpi in IFNAR blocked-infected group (Fig. 7d). The IL-1β expression levels were low during the initial days of infection up to 5 dpi. The expression levels were high during 7–15 dpi and peak expression was
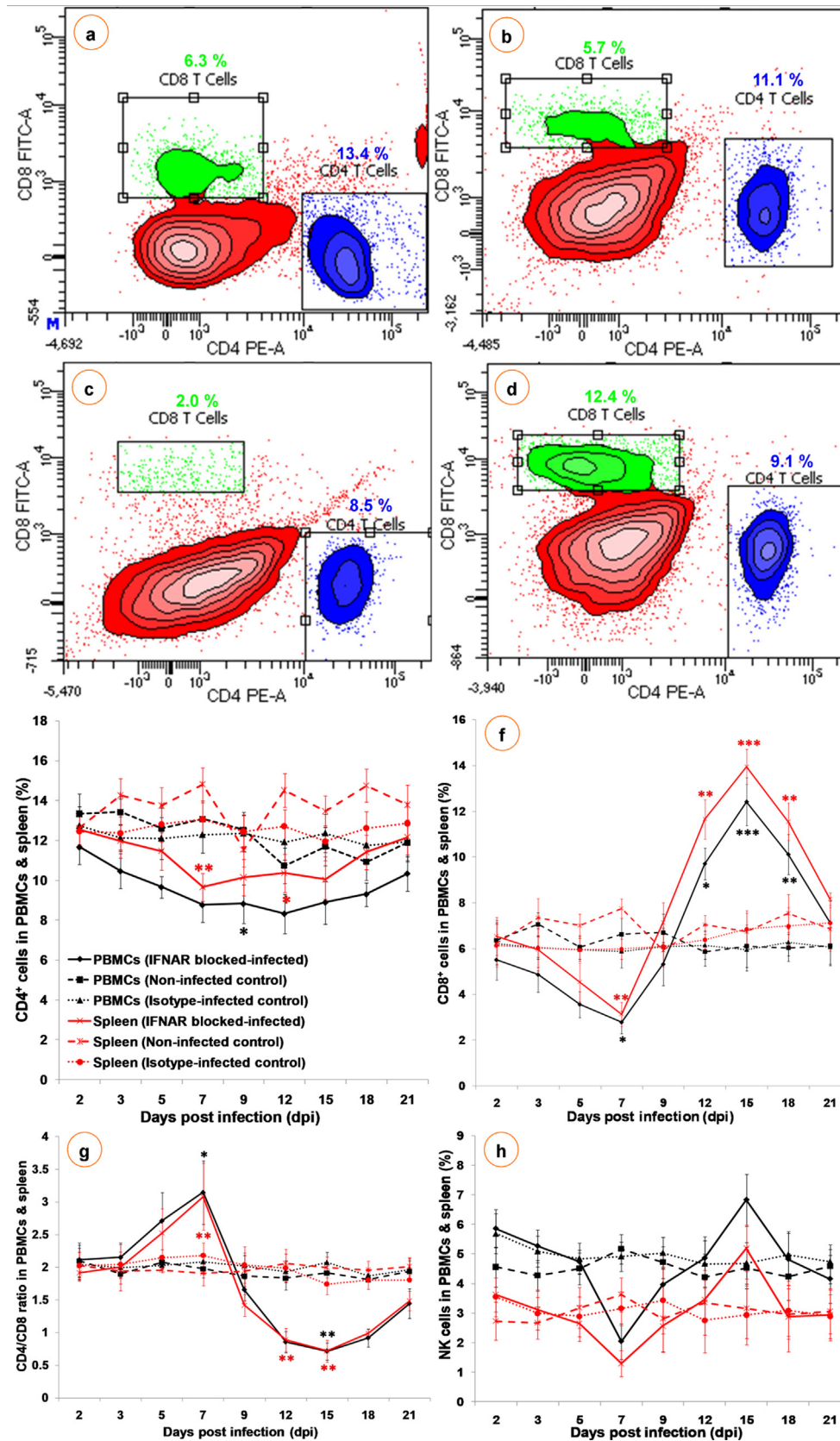
Fig. 6. Dot-plot showing flow cytometric analysis of CD4+ and CD8+ T lymphocytes after staining with PE and FITC, respectively in non-infected control (a) and IFNAR blocked-infected (b–d) groups at 5 (a, b), 7 (c) and 15 (d) dpi (n = 3). Representative figures of two independent experiments are shown. Lower right quadrant (FL2-H) represents CD4+ T lymphocytes (PE) and upper left quadrant (FL1-H) shows CD8+ T lymphocytes (FITC). (e–f) Effect of BTV-1 infection on immune cell kinetics at various time points. The IFNAR blocked-infected (solid line), isotype-infected control (round dotted line) and non-infected control (square dotted line) groups of PBMCs (black) and spleen (red). Results are presented as line diagram with mean ± SEM at each time point (n = 3). Two-way ANOVA with Bonferroni post-test was used. *P < 0.05, **P < 0.01 and ***P < 0.001 statistically significant compared with non-infected control group.
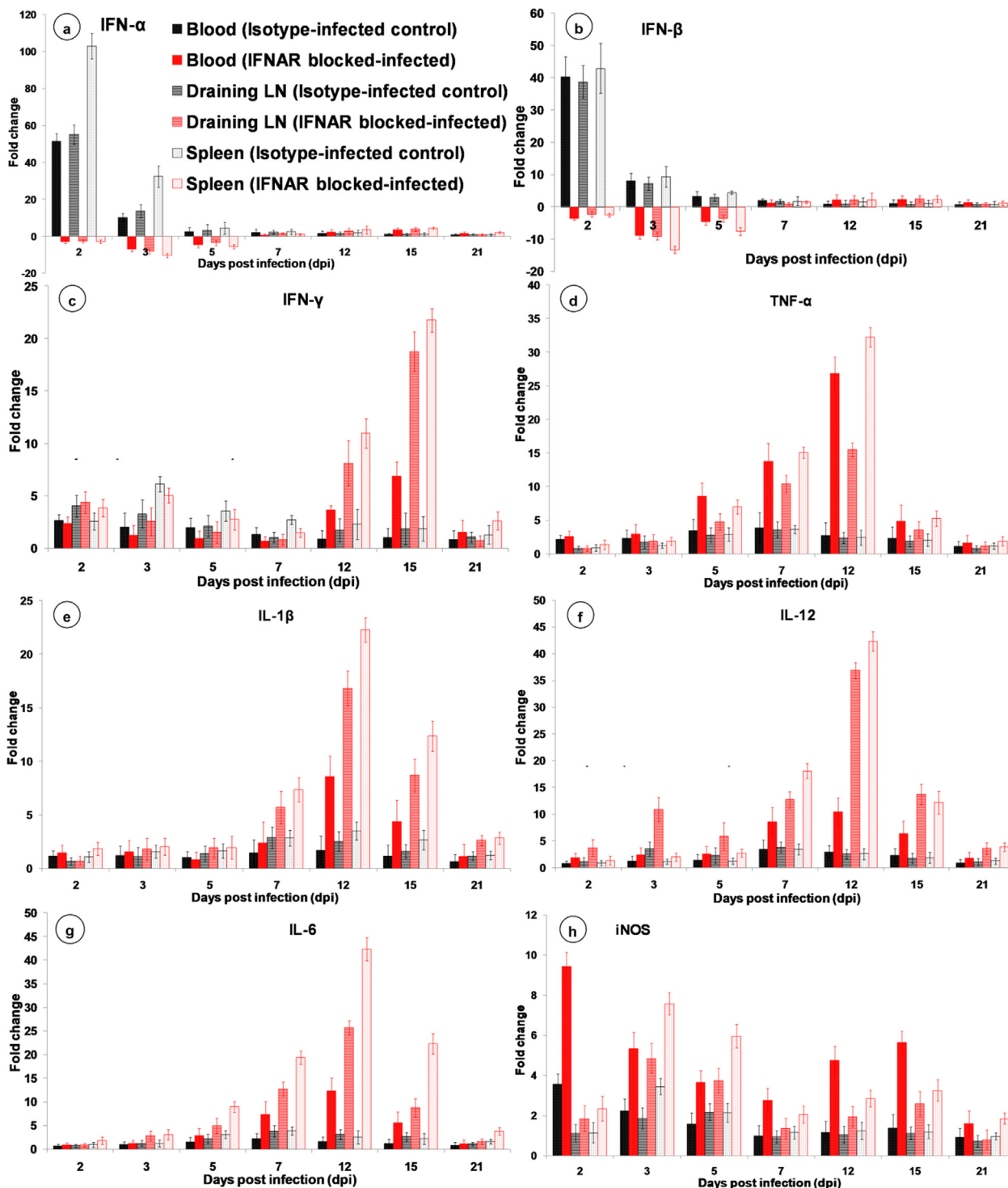
Fig. 7. Quantification of cytokine genes expressions in blood, draining LN and spleen by qRT-PCR in IFNAR blocked-infected (red bars) and isotype-infected control (black bars) groups compared to non-infected control group at various time points. Results are presented as bar diagram with mean ± SEM at each time point (n = 3).

observed at 12 dpi (Fig. 7e). The IL-12 expressions were low in PBMCs and spleen up to 5 dpi and moderate in draining LNs. The expression levels were high during 7–15 dpi and peak expression was observed at 12 dpi in IFNAR blocked-infected group (Fig. 7f).

The mRNA expressions of IL-6 increased steadily from 2–12 dpi and peak expressions were observed at 12 dpi, while the expression started to decrease from 15 dpi onward in IFNAR blocked-infected group (Fig. 7g). The mRNA expression of iNOS was high during the early stages of infection and started to decrease at 5

and 7 dpi in IFNAR blocked-infected group. Again, the expression levels of iNOS increased moderately at 12 and 15 dpi in IFNAR blocked-infected group (Fig. 7h). The FasL expression was low at 2 dpi and increased constantly from 3–12 dpi, while it reached a peak at 7 dpi in IFNAR blocked-infected group (Fig. 8d).

Analysis of apoptotic cells in PBMCs

The percentage of apoptotic cells in PBMCs were significantly (P < 0.001) increased from 3–7 dpi, levels were significantly high
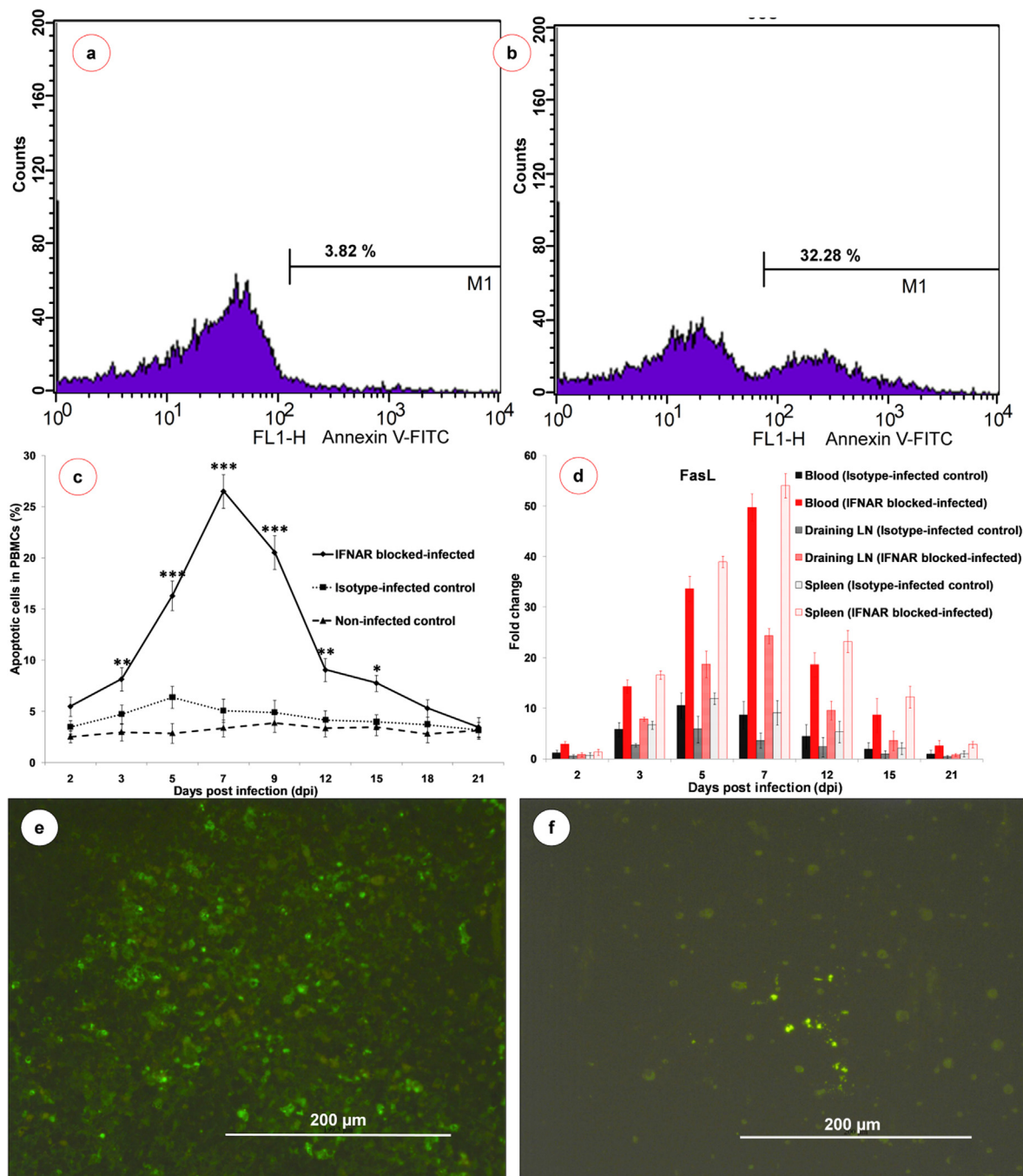
Fig. 8. Representative histogram showing the flow cytometric analysis of Annexin V-FITC staining in non-infected control (a) and IFNAR blocked-infected (b) groups at 7 dpi (n = 3). Marker M1 in the histogram represents the percentage of early apoptotic cells population. (c) Line diagram showing the percentage of early apoptotic cells in IFNAR blocked-infected (solid line), isotype-infected control (round dotted line) and non-infected control (square dotted line) groups. Results are presented as mean ± SEM at each time point (n = 3). Two-way ANOVA with Bonferroni post-test was used. *$P < 0.05$, **$P < 0.01$ and ***$P < 0.001$ statistically significant compared with control group. (d) Quantification of FasL gene expressions in blood, draining LN and spleen by qRT-PCR in IFNAR blocked-BTV infected (red bars) and isotype-infected control (black bars) groups compared to non-infected control group at various time points (n = 3). (e) Apoptotic cells showed green fluorescence signals in spleen at 7 dpi (n = 3). FITC, scale bar 200 μm. (f) Apoptotic cells showed green fluorescence signals in lungs at 7 dpi (n = 3). FITC, scale bar 200 μm.

up to 15 dpi and peak values were observed at 7 dpi in the IFNAR blocked-infected group than isotype-infected and non-infected control groups (Fig. 8b, c). The isotype-infected control group showed non-significantly high levels up to 5 dpi (Fig. 8c). The non-infected control group did not show any significant changes in the percentage of apoptotic cells in PBMCs throughout the experiment (Fig. 8a, c).

In situ detection of apoptotic cells in tissues

Apoptotic cells were detected in tissue sections of LNs, spleen (Fig. 8e), lungs (Fig. 8f), cerebrum, and cerebellum. Apoptotic signals were detected mainly from 5–12 dpi; however, more apoptotic cell signals were detected at 5–9 dpi in LNs and spleen followed by lungs when compared to other organs. The isotype-

infected and non-infected control animals showed few apoptotic cells in all these organs.

Hematological parameters

The IFNAR blocked-infected group showed decreased RBCs and Hb values at 7 dpi than isotype-infected and non-infected control groups. Significantly ($P < 0.01$) decreased RBCs values were noticed at 5 and 7 dpi and Hb at 7 dpi, and the levels were increased from 9 dpi onward and became normal, as in the isotype-infected and non-infected control groups at 21 dpi (Supplementary Fig. 5d, e). The TPC and PCV values decreased non-significantly at 7 and 9 dpi, respectively, in IFNAR blocked-infected group than isotype-infected and non-infected control groups (Supplementary Fig. 5f, h). Thereafter, the levels in IFNAR blocked-infected group started to increase and became the same as those of the control groups at 21 dpi. Further, MCV and MCHC values were in the normal range and did not reveal significant changes in IFNAR blocked-infected group than isotype-infected and non-infected control groups throughout the experiment (Supplementary Fig. 5g). No specific trend was noticed in the hematological values of isotype-infected and non-infected control groups.

Serum biochemical parameters

The SGOT, SGPT, ALP and CK values increased significantly in the IFNAR blocked-infected group compared to isotype-infected and non-infected control groups (Supplementary Fig. 7a–d). The AST values increased significantly from 7–12 dpi, with a peak increase on 9 dpi in IFNAR blocked-infected group. The ALT values also increased significantly from 5–12 dpi with a peak increase seen at 9 dpi. The ALP values ($P < 0.05$) increased significantly from 3–12 dpi with a peak increase at 7 dpi in IFNAR blocked-infected group. The CK values revealed a significantly increased trend from 5–12 dpi with a peak increase at 9 dpi in IFNAR blocked-infected group. No significant changes were noticed in the serum biochemical values of isotype-infected and non-infected control groups (Supplementary Fig. 7a–d).

Discussion

Ruminants are natural host species used for studying the pathogenesis and testing of vaccines against BT [1–4,30,31]. However, the drawbacks of conducting experimental infection studies in ruminants include the high cost, stringent ethical issues, inclusion of few animals during experimentation, difficulty in availing BTV seronegative animals in endemic areas, a longer duration of time needed for the study, and the requirement of insect vector-proof housing with BSL-3 [4–7]. To overcome these constraints, an alternative animal model is an adult mouse model because of its easy availability and manageability [7].

The present study investigated the clinico-pathological and immune responses to BTV infection in IFNAR1-blocked wild-type adult mouse. Intraperitoneal administration of IFNAR1-blocking antibody in wild-type adult mice resulted in susceptibility to BTV infection and showed clinical signs. Previous studies characterizing this antibody have reported that the half-life of 2.5 mg is 5.2 days and of 0.25 mg is 1.5 days [14,16,17]. The clinical manifestations were similar to those reported in earlier studies in IFNAR$^{(-/-)}$ mice [4–6,10,32,33]. In the present study, a lower rate of mortality was noticed at prolonged intervals than the early mortality and abnormally severe clinical disease in IFNAR$^{(-/-)}$ mice infected with BTV-1, -4, and -8, which is undesirable to study the efficacy of vaccines and immune responses against BTV [5,6,32,33].

The BTV-induced apoptosis plays a major role in the pathogenesis of BT. Several studies have shown that BTV induces apoptosis through various mechanisms [30,34,35]. It has been reported that BTV induces apoptosis through caspase-8-dependent extrinsic and caspase-9-dependent intrinsic pathways [34,35]. In the present study, apoptosis was confirmed by microscopically "starry-sky pattern" with marked lymphoid depletion, apoptosis of PBMCs by FACS, upregulation of *FasL* gene expression, and *in situ* detection of apoptotic cells in various tissues. Further, the onset of apoptosis was coincided with marked leukopenia and lymphopenia, decreased number of CD8$^+$ T cells and high virus titers. The Fas is a member of the TNF-α family, which interacts with FasL resulted in stimulation of death-signaling pathway. In the present study, FasL upregulation indicated that FasL-mediated apoptosis could be one of the mechanisms responsible for BTV induced lymphoid depletion. It is documented that FasL mRNA is up-regulated during viral infections and is responsible for evasion of the virus from the host's immune system [36]. To our knowledge, this is the first study to confirm the role of FasL-dependent apoptosis in BTV pathogenesis.

The pro-inflammatory cytokine TNF-α secreted during BTV infection has been involved in the triggering of apoptosis by increasing the transcription of TNF-α related apoptosis inducing ligand (TRAIL) [30]. Further, TNF-α induces the extrinsic pathway of apoptosis via activation of caspase-8, an apoptotic mechanism that has been reported by Umeshappa et al. [30] and Mortola and Larsen [34] during BTV-23 and BTV-10 infections in sheep. In the present study, upregulation of TNF-α levels were noticed. One possible explanation for lymphoid depletion is replication of BTV in lymphocytes, DCs, monocytes/macrophages and stem cells of the haemopoietic system, and the subsequent apoptosis and death of these infected leucocytes [2,30,34,35,37,38]. The *in vitro* susceptibility of T lymphocyte subpopulations to BTV infection has been previously described [37]. In the present study, BTV antigen was demonstrated in the LNs and spleen by IHC and qRT-PCR during the early days of infection. These findings were consistent with earlier observations in sheep and goats naturally infected with BTV [4,30,31]. In the present study, apoptosis of PBMCs with depletion of CD8$^+$ T cells and leukopenia at 7 dpi were similar to the experimental infections in sheep with BTV-1, -8 and -23, and white-tailed deer and cattle with BTV-17 [30,39–41], IFNAR$^{(-/-)}$ mouse with BTV-4 [32], and IFNAR1-blocked pregnant mouse with BTV-1 [17] have been reported earlier.

In the present study, bronchopneumonia with neutrophilic infiltration in the lungs was observed. The BTV-induced lymphoid depletion resulted in immunosuppression, which led to the predisposition of mice to secondary microbial infections [30,33,39]. Umeshappa et al. [30] have reported the complication of Pasteurella-induced pneumonia in BTV infected sheep due to immunosuppression. Calvo-Pinilla et al. [14] and Marin-Lopez et al. [32] have reported the neutrophilic infiltration in spleen of IFNAR$^{(-/-)}$ mice infected with BTV. Lungs are rich source of endothelial cells, which are an important site for BTV replication, resulted necrosis might have destroyed the antimicrobial barrier of the lungs that may have led to a favorable environment for the establishment of secondary microbial infections [30]. Studies have reported that after hemorrhage, transforming growth factor-beta (TGF-β) can be released, which can act as a mediator for host immunosuppression [42]. This may also be the cause of BTV-induced immunosuppression because hemorrhages are common during BTV infection.

The role of T lymphocyte subsets and cytokines in the regulation of humoral and cell-mediated immune responses in IFNAR blocked-infected mice has not been studied in much detail so far. The CMI plays a vital role in controlling the intracellular pathogens including viruses [40,41]. Based on literature search, the present study is the first to characterize the immune responses (kinetics

of CD4$^+$ and CD8$^+$ T cells in PBMCs and spleen) in IFNAR1-blocked wild-type adult mice infected with BTV-1. In the present study, hyperplasia of lymphoid follicles with germinal center formation, peak antibody levels, leukocytosis along with significantly increased CD4$^+$ and CD8$^+$ T cells were observed during the later stage of infection, which was possibly due to BTV-induced antigenic stimulation resulted in activation and subsequent proliferation of immune cells leading to high humoral and CMI responses. The immune cell kinetics in the present study were similar to earlier observations in natural host cattle and sheep infected with BTV [30,40,41,43] and BTV-infected-IFNAR1-blocked pregnant mice [17]. The CD8$^+$ T cells are responsible for elimination of cells infected with virus by membranolytic and secretory pathways through perforin and granzyme, and the non-secretory receptor mediated pathways involving Fas. The CD8 T cells also secrete several antiviral cytokines such as IFN-α and TNF [44].

The NK cells play a key role during viral infections through the release of chemokines and cytokines [17,45]. In the present study, increased NK cells during the later stage of infection may be activated by increased protein and mRNA expression levels of type I IFNs and IL-12. Major cytokines involved in NK cell activation are type I IFNs and IL-12 [45]. The IFNAR1-blocking resulted in activation of NK cells by type I IFNs was not possible during early days of infection. Further, IL-12 protein and mRNA expression levels were low during early days of infection. In the present study, high levels of IFN-γ during later stages of infection might have secreted by activated NK cells and associated with high CD4$^+$ and CD8$^+$ T cells ratio. During BTV infection, IL-12 is produced by DCs and other antigen-presenting cells in LNs and spleen [30,38,41,43]. The IFN-γ is secreted by cytotoxic T cells (CTLs), NK cells, DCs and Th1 cells, and responsible for the induction of virus-specific adaptive immune responses [38,40,41].

In the present study, lesions such as congestion, swollen endothelial cells, edema, and hemorrhages were observed in the visceral organs. Further, BTV antigen was demonstrated in endothelial cells of lungs, liver and brain of infected mice, suggesting virus replication in these cells. The BTV-induced vascular lesions in various organs correlated with the mRNA levels of iNOS. These results were consistent with the earlier findings of Umeshappa et al. [46] in sheep infected with BTV-23. These lesions in IFNAR blocked-infected mice were in concurrence with the lesions reported in ruminants [2,3,43]. Endothelial cells act as primary targets of BTV replication, and lesions have occurred due to vascular injury, resulting in increased vascular permeability, hemorrhages, edema, vascular thrombosis, and intense inflammation due to release of inflammatory cytokines and vasoactive mediators from BTV infected cells [2–4]. Pro-inflammatory cytokines at optimal levels act as significant molecules in the control of several viral diseases, including BTV and activation of adaptive immune responses; however, it may also damage the tissues in excess levels [31,43,46]. Various *in vitro* and *in vivo* experiments have reported that BTV infected endothelial cells, DCs, macrophages/monocytes, lymphocytes, and other cell types produce various pro-inflammatory cytokines, including IFN-α, IFN-β, IFN-γ, IL-1β, TNF-α, IL-4, IL-6, IL-8, IL-10, IL-12, NOS, and iNOS, which may be responsible for pathogenesis of BT [30,31,38,41,43,46].

The level of enzymes in the serum indirectly indicates its amount in the cell, degree of cell damage, and necrosis [47]. In the present study, significantly increased serum levels of AST, ALT, ALP, and CK enzymes indicated BTV-induced damage to soft tissues such as lymphoid organs, lungs, heart, skeletal muscle, brain, kidneys, and liver. These findings were agree with the previous findings in sheep infected with BTV [48]. The AST is a marker for soft tissue damage and both ALT and AST are the significant markers for hepatocellular damage. Though ALP is present in all tissues, the greater activity of this enzyme is seen in the kidneys,

liver and intestinal tissues. Increased CK enzyme levels indicated BTV-induced degeneration and necrosis of brain, cardiac and skeletal muscles [48]. Aytekin et al. [49] reported that BTV induced lipid peroxidation was responsible for elevated levels of these enzymes in the serum.

In the present study, significantly decreased values of RBCs, Hb, PCV, and platelets (thrombocytopenia) were observed at 7 dpi. It is well known that BTV attached to erythrocytes results in destruction of RBCs leading to anemia [48]. It is reported that BTV replicates in circulating platelets and megakaryocytes during the viremic stage, resulting in thrombocytopenia [40]. Further, BTV-induced widespread hemorrhages may also be responsible for the sequestration of RBCs and platelets in vascular lesions resulting in anemia and thrombocytopenia.

Conclusions

The present study is the first to characterize an immunocompetent adult mouse model with type I IFNs blockade at the time of BTV infection. The isotype-infected control mice did not develop any disease; whereas, IFNAR blocked-infected mice developed clinical signs and typical lesions of BT like lymphoid depletion in lymph nodes and spleen, interstitial pneumonia and haemorrhages in various organs. Disease progression, pathogenesis and immune responses were closely mimicked as that of natural BTV infection in ruminants. This mouse model is suitable for studying BTV transmission, virulence, pathogenesis, immune responses, and testing the protective efficacy of BTV vaccines. However, extrapolation of the results in mouse to ruminants should be given due consideration due to differences in the ruminant and mouse biology.

Declaration of Competing Interest

The authors declare that they have no known competing financial interests or personal relationships that could have appeared to influence the work reported in this paper.

Acknowledgements

Appendix A. Supplementary material

Supplementary data to this article can be found online at https://doi.org/10.1016/j.jare.2021.01.007.

References

[1] Saminathan M, Singh KP, Khorajiya JH, Dinesh M, Vineetha S, Maity M, et al. An updated review on Bluetongue virus: Epidemiology, pathobiology, and advances in diagnosis and control with special reference to India. Vet Q 2020;40:258–321.

[2] Maclachlan NJ, Drew CP, Darpel KE, Worwa G. The pathology and pathogenesis of bluetongue. J Comp Pathol 2009;141:1–16.

[3] Maclachlan NJ, Crafford JE, Vernau W, Gardner IA, Goddard A, Guthrie AJ, et al. Experimental reproduction of severe bluetongue in sheep. Vet Pathol 2008;45:31–315.

[4] Coetzee P, van Vuuren M, Venter EH, Stokstad MA. Review of experimental infections with bluetongue virus in the mammalian host. Virus Res 2014;182:21–34.

[5] Calvo-Pinilla E, Rodriguez-Calvo T, Anguita J, Sevilla N, Ortego J. Establishment of a bluetongue virus infection model in mice that are deficient in the alpha/beta interferon receptor. PLoS ONE 2009;4:e5171.

[6] Ortego J, de la Poza F, Marin-Lopez A. Interferon α/β receptor knockout mice as a model to study bluetongue virus infection. Virus Res 2014;182:35–42.

[7] Saminathan M, Singh KP, Rajasekar R, Malik YPS, Dhama K. Role of type I interferons in the pathogenesis of bluetongue virus in mice and ruminants. J Exp Biol Agric Sci 2019;7:513–20.

[8] Saminathan M, Singh KP, Vineetha S, Maity M, Biswas SK, Reddy GBM, et al. Factors determining the clinical outcome of bluetongue virus infection in adult mice. Indian J Vet Pathol 2018;42:239–48.

[9] Jameson P, Schoenherr CK, Grossberg SE. Bluetongue virus, an exceptionally potent interferon inducer in mice. Infect Immun 1978;20:321–3.

[10] Vitour D, Doceul V, Ruscanu S, Chauveau E, Schwartz-Cornil I, Zientara S. Induction and control of the type I interferon pathway by bluetongue virus. Virus Res 2014;182:59–70.

[11] Brewer AW, Osburn BI. Sequential distribution of neurovirulent and avirulent strains of bluetongue virus in neonatal mice by RT-PCR. Arch Virol 1998;143:145–55.

[12] Anjaneya A, Singh KP, Cherian S, Saminathan M, Singh R, Ramakrishnan MA, et al. Comparative neuropathology of major Indian bluetongue virus serotypes in a neonatal BALB/c mouse model. J Comp Pathol 2018;162:18–28.

[13] Narayan O, Johnson RT. Effects of viral infection on nervous system development. I. Pathogenesis of bluetongue virus infection in mice. Am J Pathol 1972;168:1–14.

[14] Sheehan KC, Lai KS, Dunn GP, Bruce AT, Diamond MS, Heutel JD, et al. Blocking monoclonal antibodies specific for mouse IFN-alpha/beta receptor subunit 1 (IFNAR-1) from mice immunized by *in vivo* hydrodynamic transfection. J Interferon Cytokine Res 2006;26:804–19.

[15] Sheehan KCF, Lazear HM, Diamond MS, Schreiber RD. Selective blockade of interferon-α and -β reveals their non-redundant functions in a mouse model of West Nile virus infection. PLoS ONE 2015;10:e0128636.

[16] Smith DR, Hollidge B, Daye S, Zeng X, Blancett C, Kuszpit K, et al. Neuropathogenesis of Zika virus in a highly susceptible immunocompetent mouse model after antibody blockade of type I interferon. PLoSNegl Trop Dis 2017;11:e0005296.

[17] Saminathan M, Singh KP, Vineetha S, Maity M, Biswas SK, Manjunathareddy GB, et al. Virological, immunological and pathological findings of transplacentally transmitted bluetongue virus serotype 1 in IFNAR1-blocked mice during early and mid gestation. Sci Rep 2020;10:2164.

[18] Chauhan HC, Biswas SK, Chand K, Rehman W, Das B, Dadawala AI, et al. Isolation of bluetongue virus serotype 1 from aborted goat fetuses. Rev Sci Tech 2014;33:803–12.

[19] Jabbar TK, Calvo-Pinilla E, Mateos F, Gubbins S, Bin-Tarif A, Bachanek-Bankowska K, et al. Protection of IFNAR(−/−) mice against bluetongue virus serotype 8, by heterologous (DNA/rMVA) and homologous (rMVA/rMVA) vaccination, expressing outer-capsid protein VP2. PLoS ONE 2013;8: e60574.

[20] Marin-Lopez A, Calvo-Pinilla E, Barriales D, Lorenzo G, Brun A, Anguita J, et al. CD8 T cell responses to an immunodominant epitope within the nonstructural protein NS1 provide wide immunoprotection against bluetongue virus in IFNAR−/− Mice. J Virol 2018;92:e00938–1018.

[21] Lakshmi IK, Putty K, Raut SS, Patil SR, Rao PP, Bhagyalakshmi B, et al. Standardization and application of real time polymerase chain reaction for rapid detection of bluetongue virus. Vet World 2018;11:452–8.

[22] McCarthy MK, Procario MC, Twisselmann N, Wilkinson JE, Archambeau AJ, Michele DE, et al. Proinflammatory effects of interferon gamma in mouse adenovirus 1 myocarditis. J Virol 2015;89:468–79.

[23] McKimmie CS, Johnson N, Fooks AR, Fazakerley JK. Viruses selectively upregulate Toll-like receptors in the central nervous system. BiochemBiophys Res Commun 2005;336:925–33.

[24] Samuel MA, Diamond MS. Alpha/beta interferon protects against lethal West Nile virus infection by restricting cellular tropism and enhancing neuronal survival. J Virol 2005;79:13350–61.

[25] Chen J, Yuan L, Fan Q, Su F, Chen Y, Hu S. Adjuvant effect of docetaxel on the immune responses to influenza A H1N1 vaccine in mice. BMC Immunol 2012;13:36.

[26] Allam R, Scherbaum CR, Darisipudi MN, Mulay SR, Hagele H, Lichtnekert J, et al. Histones from dying renal cells aggravate kidney injury via TLR2 and TLR4. J Am Soc Nephrol 2012;23:1375–88.

[27] Li X, Jin Q, Yao Q, Xu B, Li L, Zhang S, et al. The flavonoid quercetin ameliorates liver inflammation and fibrosis by regulating hepatic macrophages activation and polarization in mice. Front Pharmacol 2018;9:72.

[28] Doi SQ, Jacot TA, Sellitti DF, Hirszel P, Hirata MH, Striker GE, et al. Growth hormone increases inducible nitric oxide synthase expression in mesangial cells. Am Soc Nephrol 2000;11:1419–25.

[29] Ubol S, Kasisith J, Pitidhammabhorn D, Tepsumethanol V. Screening of proapoptotic genes upregulated in an experimental street rabies virus-infected neonatal mouse brain. Microbiol Immunol 2005;49:423–31.

[30] Umeshappa CS, Singh KP, Nanjundappa RH, Pandey AB. Apoptosis and immuno-suppression in sheep infected with bluetongue virus serotype-23. Vet Microbiol 2010;144:310–8.

[31] Sanchez-Cordon PJ, Pedrera M, Risalde MA, Molina V, Rodriguez-Sanchez B, Nunez A, et al. Potential role of pro-inflammatory cytokines in the pathogenetic mechanisms of vascular lesions in goats naturally infected with bluetongue virus serotype 1. Transbound Emerg Dis 2013;60:252–62.

[32] Marin-Lopez A, Bermudez R, Calvo-Pinilla E, Moreno S, Brun A, Ortego J. Pathological characterization of IFNAR(−/−) mice infected with bluetongue virus serotype 4. Int J Biol Sci 2016;12:1448–60.

[33] Calvo-Pinilla E, Nieto JM, Ortego J. Experimental oral infection of bluetongue virus serotype 8 in type I interferon receptor-deficient mice. J Gen Virol 2010;91:2821–5.

[34] Mortola E, Larsen A. Bluetongue virus infection: signaling pathway activated during apoptosis. Rev Argent Microbiol 2009;41:134–40.

[35] Nagaleekar VK, Tiwari AK, Kataria RS, Bais MV, Ravindra PV, Kumar S. Bluetongue virus induces apoptosis in cultured mammalian cells by both caspase dependent extrinsic and intrinsic apoptotic pathways. Arch Virol 2007;152:1751–6.

[36] Madhu BP, Singh KP, Saminathan M, Singh R, Tiwari AK, Manjunatha V, et al. Correlation of inducible nitric oxide synthase (iNOS) inhibition with TNF-α, caspase-1, FasL and TLR-3 in pathogenesis of rabies in mouse model. Virus Genes 2016;52:61–70.

[37] Takamatsu H, Mellor PS, Mertens PP, Kirkham PA, Burroughs JN, Parkhouse RM. A possible overwintering mechanism for bluetongue virus in the absence of the insect vector. J Gen Virol 2003;84:227–35.

[38] Hemati B, Contreras V, Urien C, Bonneau M, Takamatsu H-H, Mertens PPC, et al. Bluetongue virus targets conventional dendritic cells in skin lymph. J Virol 2009;83:8789–99.

[39] Barratt-Boyes SM, Maclachlan NJ. Pathogenesis of bluetongue virus infection of cattle. J Am Vet Med Assoc 1995;206:1322–9.

[40] Ellis JA, Luedke AJ, Davis WC, Wechsler SJ, Mecham JO, Pratt DL, et al. T lymphocyte subset alterations following bluetongue virus infection in sheep and cattle. Vet Immunol Immunopathol 1990;24:49–67.

[41] Sanchez-Cordon PJ, Perez de Diego AC, Gomez-Villamandos JC, Sanchez-Vizcaino JM, Pleguezuelos FJ, Garfia B, et al. Comparative analysis of cellular immune responses and cytokine levels in sheep experimentally infected with bluetongue virus serotype 1 and 8. Vet Microbiol 2015;177:95–105.

[42] Ayala A, Meldrum DR, Perrin MM, Chaudry IH. The release of transforming growth factor-beta following haemorrhage: its role as a mediator of host immunosuppression. Immunology 1993;79:479–84.

[43] Channappanavar R, Singh KP, Singh R, Umeshappa CS, Ingale SL, Pandey AB. Enhanced proinflammatory cytokine activity during experimental bluetongue virus-1 infection in Indian native sheep. Vet Immunol Immunopathol 2012;145:485–92.

[44] Kulinski JM, Tarakanova VL, Verbsky J. Regulation of antiviral CD8 T-cell responses. Crit Rev Immunol 2013;33:477–88.

[45] Paolini R, Bernardini G, Molfetta R, Santoni A. NK cells and interferons. Cytokine Growth Factor Rev 2015;26:113–20.

[46] Umeshappa CS, Singh KP, Nanjjundappa RH, Channappanavar R, Maan S, Mann NS. Bluetongue virus-23 stimulates inducible nitric oxide synthase expression and nitric oxide production in mononuclear cells of blood and/or regional lymphoid organs. Vet Res Commun 2012;36:245–50.

[47] Tothova C, Nagy O, Kovac G. Serum proteins and their diagnostic utility in veterinary medicine: a review. Vet Med – Czech 2016;61:475–96.

[48] Sobharani V, Singh KP, Maity M, Sharma GK, Saminathan M, Sahoo D, et al. Comparative study on hemato-biochemical alterations and selected acute phase protein response in native sheep experimentally infected with bluetongue virus serotypes 10 and 24. Comp Clin Pathol 2019;28:1153–63.

[49] Aytekin I, Aksit H, Sait A, Kaya F, Aksit D, Gokmen M, et al. Evaluation of oxidative stress via total antioxidant status, sialic acid, malondialdehyde and RT-PCR findings in sheep affected with bluetongue. Vet Rec Open 2015;2: e000054.